

Towards a Theory of Mechanochemistry – Simple Models from the Very Beginnings

Wolfgang Quapp*, Josep Maria Bofill[†] and Jordi Ribas-Ariño[‡]

July 7, 2018

Abstract

A core idea in the context of mechanochemistry is that applying an external tensile force along a reaction coordinate should enhance the chemical reaction of interest. Here we analyze perturbed generic molecular structures: schematic models of triatomics, ABC, and tetraatomics, AABB. They are used to demonstrate that pulling does usually not use the 'reaction coordinate', but opens new reaction pathways. Within development of these models we use the concept of Newton trajectories for a theory of mechanochemistry. However, we find cases where the theory of Newton trajectories is not applicable. For all cases we define the curve of force-displaced stationary points, and we discuss the importance of barrier breakdown points and valley-ridge inflection points. The examples use Morse potentials for bonds and simple angle functions and are demonstrated by assumed real values for the potential parameters. On the basis of the systematic study of some generic models we explain a set of already observed experimental mechanochemical phenomena in specific molecular systems and we apply the results to the strength of chemical bonds.

Keywords: Mechanochemistry, Force displaced stationary points, Barrier breakdown point, Valley-Ridge inflection point, Newton trajectory, Force-extension curve

1 Introduction

The study of how external mechanical forces change the potential energy surfaces (PES) of molecular systems is of highest relevance in the context of mechanochemistry because this can lead to a better understanding of the molecular level of the mechanisms by which external forces control chemical processes. In the last years, the chemical response of single molecules, polymers, covalent inorganic crystals, metals, molecular solids etc. when subjected

*Mathematisches Institut, Universität Leipzig, PF 100920, D-04009 Leipzig, Germany, quapp@uni-leipzig.de; <http://www.math.uni-leipzig.de/~quapp>

[†]Departament de Química Inorgànica i Orgànica, Secció de Química Orgànica, Universitat de Barcelona; and Institut de Química Teòrica i Computacional, Universitat de Barcelona, (IQTCUB), Martí i Franquès 1, 08028 Barcelona, Spain, jmbofill@ub.edu

[‡]Departament de Ciència de Materials i Química Física, IQTCUB, Universitat de Barcelona, Martí i Franquès 1, 08028 Barcelona, Spain, j.ribas@ub.edu

to mechanical forces has motivated experimental and theoretical researches.¹⁻²⁰ Chemical reactions can be thought of in terms of their 'landscapes' - multi-dimensional PESes with a dimension much higher than three dimensions of our usual space - that map the saddle-pathways and valleys of the potential energy as molecules interact.²¹ In 2008 Lourderaj et al.²² calculated the PES of stretched n-butane. They found that the nature of the effective PES under the stretching depends on the extent of stretching. If it is less than that required to reach the valley-ridge-inflection (VRI) points on the C-C stretch potentials and the C-C torsions are considered free rotors, then there is only one potential energy minimum, with each bond elongated. However, for stretching past these inflection points, the PES has bifurcated into three minima.

Here we do, in a framework of minimal models, a similar set of calculations for simpler schematic triatomics ABC and tetraatomics AABB molecules to demonstrate that the influence of the stretching depends not only on the magnitude but also on its direction. Thus, we study different possible directions of the force²³ in an ansatz which goes beyond the usual 1-dimensional (1D) point of view. The treatment touches the question: "How strong is a covalent bond?"²⁴⁻²⁸ or how weak is a non covalent bond.²⁹ Grandbois et al.²⁴ measured the rupture force of single covalent bonds (silicon-carbon, or gold-gold bonds) under an external load with an atomic force microscope. Single molecules were covalently anchored between a surface and a tip of the microscope and then stretched until they became detached. Our remark here is: the pulling done by the microscope usually goes over a larger part of the molecule by an end-to-end force. So in internal coordinates, this direction is usually another direction than the one along a single bond.³⁰⁻³⁴ Then the amount obtained by the microscope must be larger than the amount for a single bond to break because other bonds always absorb force as well.³⁵⁻³⁷

We use a model for the effective PES, $V_{\mathbf{f}}(\mathbf{x})$ for a fixed force, \mathbf{f} , via the approximation in \mathbf{x} ^{5,10,26,29,38-48}

$$V_{\mathbf{f}}(\mathbf{x}) = V(\mathbf{x}) - \mathbf{f}^T \cdot \mathbf{x} \tag{1}$$

where the superscript T denotes transpose, and \mathbf{x} is the vector of the non redundant, internal coordinates of the molecule. The symbolic point between \mathbf{f} and \mathbf{x} means the scalar product. This is explained elsewhere.⁴⁹ The dimension of the vectors, \mathbf{f} and \mathbf{x} , is $N = 3n - 6$ internal coordinates, and n is the number of atoms of the treated molecule. The vector of the force, \mathbf{f} , is determined by two properties: its direction and its length. If the force is constant, then we say that the model of Eq.(1) is a linear model. We can say that Eq.(1) reflects the perturbation of a molecular system due to an external force with constant direction. This perturbation changes the landscape of the original PES. The stationary points of $V_{\mathbf{f}}$ are located at different points with respect to the unperturbed potential.^{10,48,50-54} We will later see that in the limiting case of a critical force, \mathbf{f}_c , a minimum and a transition state of the original PES collapse on a shoulder of the resulting perturbed PES. Of course, the stationary points of $V_{\mathbf{f}}(\mathbf{x})$ can be calculated by usual optimization procedures, see Ref.⁵⁵ and further references therein.

For the linear model and a fixed direction \mathbf{l} of \mathbf{f} , the disturbance of the stationary points on the effective PES, $V_{\mathbf{f}}(\mathbf{x})$, can be described by Newton trajectories (NT). Then only the norm of \mathbf{f} can change.^{53,54,56-60} NTs are mathematical curves in the configuration space which can be calculated by simple mathematical methods. They allow qualitative pictures

of the change of the effective PES. In this work, we study the applicability of the theory of NTs to very small toy molecules under an external force.

In Section 2 we shortly describe the background necessary to the application of NTs. In Section 3 we introduce a Morse model for a linear molecule, and in Section 4 for a linear chain where NTs can be applied. In Section 5 we treat a bent ABA molecule. It turns out that already in this simple case the NT theory cannot be applied. Nevertheless, we calculate the corresponding curve of the force-displaced stationary points (FDSPs) for an end-to-end pulling. Here we also demonstrate the meaning of the strength of a single bond, and we discuss force-extension curves. In Sections 6 to 8 we describe further molecule models for nonlinear molecules and rings. In a last example in Section 9 we study defolding and refolding of a model hairpin by an external force. The end is a Discussion with Conclusions.

2 Application of Newton trajectories

The stationary points on the effective potential satisfy the condition, $\nabla_{\mathbf{x}} V_{\mathbf{f}}(\mathbf{x}) = \mathbf{0}$. Its minimums and saddle points (SPs) satisfy the vector equation⁴²

$$\nabla_{\mathbf{x}} V_{\mathbf{f}}(\mathbf{x}) = \mathbf{g}(\mathbf{x}) - \mathbf{f} = \mathbf{0} . \quad (2)$$

One searches a point where the gradient of the original PES, $\mathbf{g}(\mathbf{x})$, has to be equal to the force, \mathbf{f} . The gradient of $V(\mathbf{x})$ is the inner force of the molecule against changes of its structure. This force has to be equal to the external force, \mathbf{f} . Then the molecule is in an equilibrium: we are at a stationary point of $V_{\mathbf{f}}(\mathbf{x})$. However, this formula (2) is also the definition of an NT in the case that the force \mathbf{f} changes its magnitude in a continuous way but its direction remains a constant vector. Thus, the NT describes a curve of force-displaced stationary points (FDSPs) under a different load.^{53,54,56-60} Usually, the minima are destabilized, but the SPs are stabilized.^{53,54,61} Of course, we assume here that the time scale of the intra-well relaxation is faster than any other time scale of the pulling apparatus.⁶² Because the barrier in the drag direction decreases, the chemical reaction of interest usually becomes fast^{63,64} or ultra-fast.⁶⁵

Eq.(2) can be written in a projector form^{56,57}

$$(\mathbf{U} - \mathbf{l}\mathbf{l}^T) \mathbf{g}(\mathbf{x}) = \mathbf{0} \quad (3)$$

where \mathbf{U} is the unit matrix and the \mathbf{l} -unit vector is the direction of \mathbf{f} . The equation means nothing else than that \mathbf{g} and \mathbf{l} are parallel. If we differentiate the projector Eq.(3) with respect to the parameter that characterizes the curve, s , we obtain with the Hessian, \mathbf{H} ,^{57,59}

$$(\mathbf{U} - \mathbf{l}\mathbf{l}^T) \mathbf{H}(\mathbf{x}) \frac{d\mathbf{x}}{ds} = \mathbf{0} . \quad (4)$$

This is an expression of the tangent of the FDSPs curve, $\mathbf{x}(s)$. Eq.(4) is a way to generate the FDSPs curve.

Every NT connects stationary points. If one uses a given fixed unit vector of the direction, \mathbf{l} of \mathbf{f} , and if one goes along the corresponding FDSPs curve, then the magnitude of the force, $F = |\mathbf{f}|$, starts with zero at a stationary point, say a minimum, and ends with zero at the

final next stationary point, say an SP. In between there has to be a maximum of $|\mathbf{g}|$, compare Eq.(2). Here holds the condition^{10,53,63}

$$Det(\mathbf{H}(\mathbf{x})) = 0 \tag{5}$$

with the Hessian of the original PES, $V(\mathbf{x})$. The case is the point where the square of the gradient norm achieves a turning point, and the effective $V_{\mathbf{f}}(\mathbf{x})$ along the FDSPs path here achieves a shoulder^{10,53,63} which is a cubic function in 1D along the pulling direction.⁴⁰ The point on the FDSPs curve is referred to as bond breaking point (BBP)^{53,63} and the pulling force is at its 'mechanical limit'.⁴² The bond elongation comes to its maximum. The barrier of $V_{\mathbf{f}}(\mathbf{x})$ decreases from the original PES barrier to zero at the BBP thus the BBP is also the barrier breakdown point with an identical acronym, BBP. This happens because minimum and SP coalesce. The force that needs to be applied to meet the BBP on the corresponding effective PES is named the critical force, \mathbf{f}_c .⁴⁰ The kind of points is also discussed elsewhere.¹³ An algorithm to locate optimal BBPs has been recently proposed.⁶⁶ Note that a bond will actually break before the BBP due to finite temperature effects⁶⁷⁻⁶⁹ or by the zero point energy of the corresponding bond. The kinetics of the break caused mainly by the force can be explained by a usual escape of the molecular state over the decreasing barrier. However, the barrier 'last' to overcome below the BBP will be elusive, see below Sections 5 and 9. Conversely to the calculation of the BBP of a given PES,⁶⁶ there are proposals to use pulling experiments to reconstruct a one-dimensional section of the PES in the pulling direction.⁷⁰⁻⁷² However, there are also mental reservations against the possibility of such an ansatz.⁷³

3 Model PES for pulling a linear ABC molecule

We start with only two bonds, two simple Morse-potentials in a linear triatomic molecule. x is one bond and y the other one, see Fig. 1. Then we get a simple minimum at the point (x_0, y_0) . Under a global deformation of the end-to-end distance, ΔR between atoms A and C, by the force \mathbf{f} for an end-to-end pulling we search for the single deformations Δx and Δy of the two bonds. We use the following function for a 2D-section of this schematic molecule

$$\begin{aligned} M_1(x) &= D_1(1 - \exp[-\beta_1(x - x_0)])^2 \\ M_2(y) &= D_2(1 - \exp[-\beta_2(y - y_0)])^2 \\ V(x, y) &= M_1(x) + M_2(y) \end{aligned} \tag{6}$$

where the constants are slightly unsymmetrical:

$$D_1 = 90, D_2 = 80, \beta_1 = 1.8, \beta_2 = 1.9, x_0 = 1.52, y_0 = 1.53.$$

The parameters D_1 and D_2 represent the dissociation energy, but the $1/\beta_1$ and $1/\beta_2$ the width of the potentials, correspondingly, compare Ref.²² Note that Morse potentials have already been employed to model mechanochemical events, for instance, the Fe-S bond dissociation events in force-field simulations of rubredoxin unfolding Ref.⁷⁴ A third internal coordinate in the ABC molecule may be the angle, α , between the two bonds. In this case, we assume that it is fixed to 180° . In the next sections, we will consider the angle as a variable, too. The PES of Eq.(6) was purposely kept simple to understand the key features of the pulling

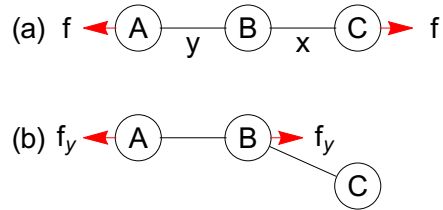


Figure 1: A schematic triatomic molecule, ABC, connected by Morse potentials. (a) Top line: the arrow \mathbf{f} is the pulling force for an end-to-end action with direction $\mathbf{l} = 1/\sqrt{2}(1, 1)^T$, but line (b) below: \mathbf{f}_y is a pulling along only one bond with $\mathbf{l}_y = (0, 1)^T$.

problem. We are interested in the study of the combined, end-to-end force \mathbf{f} of Fig. 1(a). Examples of forces like \mathbf{f}_y in Fig. 1(b) are calculated elsewhere.^{28,75} An asymmetric force in a molecule can be applied by corresponding chemical 'linkers'.⁴⁷ In Fig. 2 we show the surface of $V(x, y)$ of Eq.(6) by its contours. The figure (and all the next ones) are drawn by the Mathematica program, version 11.2. The level lines are represented equidistantly. The two valleys in Fig. 2 are only slightly different. A single Morse curve has its BBP at the value²²

$$x_{BBP} = x_o + \ln 2 / \beta_1. \quad (7)$$

Because here the two degrees of freedom are not coupled, this holds on a straight line for $x_{BBP} = x_o + 0.385 = 1.905$ and similarly for $y_{BBP} = y_o + \ln 2 / \beta_2 = y_o + 0.365 = 1.895$. The critical forces are at point (x_{BBP}, y_0) the force $\mathbf{f}_c = 81(1, 0)^T$ and at point (x_0, y_{BBP}) the force $\mathbf{f}_c = 76.1(0, 1)^T$. The green lines in Fig. 2 correspond to these BBPs of the two valleys. They intersect in a VRI point of the surface.^{53,54,63} Here the normalized gradient vector, an eigenvector of the Hessian matrix at this VRI point, is $\mathbf{g}_W = W(D_1\beta_1, D_2\beta_2)^T$ with eigenvalue zero and its orthogonal eigenvector with zero eigenvalue is $\mathbf{g}_W^\perp = W(D_2\beta_2, -D_1\beta_1)^T$, where W is the normalization factor, $W = (D_1^2\beta_1^2 + D_2^2\beta_2^2)^{-1/2}$. The lines are characterized by the condition of Eq.(5). In Fig. 2, additionally included are the lines (thin, gray) of the two NTs along the valleys, NT_x and NT_y , to the pulling directions $\mathbf{l}_x = (1, 0)^T$ and $\mathbf{l}_y = (0, 1)^T$. The latter direction is shown in Fig. 1(b).

3.1 Step one: pulling symmetrically a triatomic molecule with $\mathbf{f} = 25(1, 1)^T$

We apply the same force to the outer atoms A and C of the ABC system, but in opposite direction. Both bonds are stretched. The force vector is $\mathbf{f}^T = -25(1, 1)$ with modulus $|\mathbf{f}| = 25\sqrt{2}$ units of force, see Fig. 3. We assume that the disturbed molecule immediately moves into the new, effective minimum. It will be on the NT $\mathbf{x}(s)$ named $\text{NT}_{1,1}$. The resulting effective potential, obtained by the application of Eq.(1) is reported in Fig. 3. On this PES the FDSP located in the y -direction, namely SP_y , is at -42.27 units of Eq.(6) at point (1.57, 2.8). The SP in the x -direction is also lowered. This stationary point is energetically nearby at -35.73 units at point (2.89, 1.58), see Fig. 3. The reason of this behavior is due to the fact that the applied force points indeed in the combination direction where the VRI point is nearby located, that is along the direction of the straight line $y = x$. In other words,

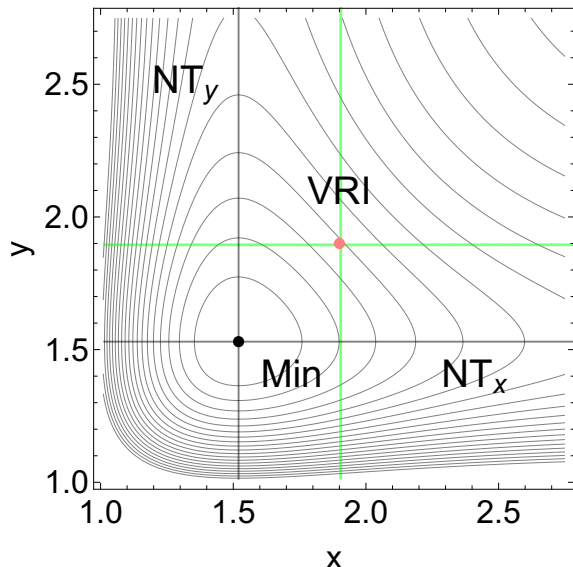


Figure 2: A nearly symmetric, 2D-Morse potential. Lines of BBPs are green. VRI is the valley-ridge inflection point. Two NTs (gray) form the minimum energy pathways along the dissociation valleys.

both axes directions are involved in \mathbf{f} and both SPs undergo a TS stabilization.^{61,76} Note that also the minimum suffers a little destabilization. It also moves along the $\text{NT}_{1,1}$.

Regarding Eq.(6) we see that the PES is not totally symmetric, the SP_y is less energetical than SP_x . This implies that the AB bond is a little weaker than the BC bond, the energy barrier from the minimum to the SP_y is the lowest. We emphasize that the symmetric force lowers both TSs as one would expect it.

Now the following question arises: is the above symmetric force the optimal one to break a bond, say y between AB? If it is not then how to find out and characterize it? This is an important question for both theory and applied mechanochemistry. From an intuitive point of view, taking the central atom B and the outer atom A under force and relaxing the atom C, like in Fig. 1(b), the applied force will break the AB bond in the easiest way. The AB bond is parallel to the y -axis, which is the direction where the reaction valley between the minimum and the lowest SP is located. Thus, a pulling which acts along the y -direction should meet the lowest energy barrier.

An interesting feature of the PES given in Eq.(6), see also Fig. 2, is that each reaction valley corresponds to a bond breaking process. As noted above in the direction of the y -axis, the valley is associated to the AB bond breaking but the BC bond remains. In the opposite case one can take the x -axis direction. The border point of this behavior is near the straight-line, $y = x$, the VRI point.²²

It is known that different directions of an outer force can change the kind of the reaction path.^{23,41,43,53,54,77-81} This one applied to our model system means that the external force could be applied either in the x - or in the y -direction. However, pulling along the symmetric $\mathbf{l}_{1,1} = 1/\sqrt{2}(1, 1)^T$ -direction is characterized by a slightly un-symmetric NT, shown in Fig. 3 by the blue curves. It avoids a direct crossing of the VRI point. Its $\text{BBP}_{1,1}$, however, is also shown in Fig. 3, see further effective PESes of this special $\text{BBP}_{1,1}$ below.

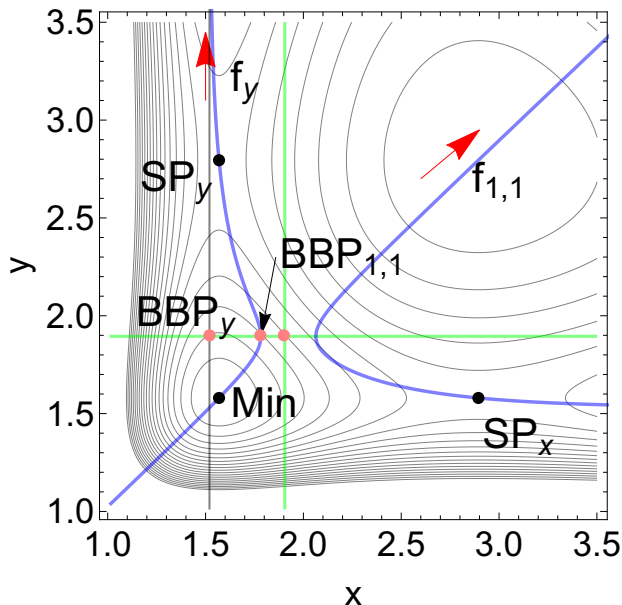


Figure 3: The effective 2D-Morse potential with $\mathbf{f}_{1,1} = 25(1, 1)^T$. The gray line is the NT along the former MEP of the y -valley, the blue curve is the NT to direction $\mathbf{f}_{1,1}$ which leads near the VRI point to the crossing of the green lines of BBPs. On this NT all stationary points move thus, it is the curve of FDSPs. The BBPs do not change under $\mathbf{f}_{1,1}$. For comparison we add the BBP_y and the \mathbf{f}_y which are not in use here.

The left branch of the $\text{NT}_{1,1}$ connects the minimum with the SP_y , its right branch connects the SP_x with the maximum of the effective PES, an SP of index two. (It is an important property of NTs to connect stationary points with an index difference of 1, see Ref.⁸²) The left curve of the $\text{NT}_{1,1}$ will lead to a coalescence of minimum and the SP_y for a high enough pulling force at $\text{BBP}_{1,1}$, shown below.

Figure 4(a) depicts a comparison of the gradient norms of the original PES of Eq.(6) over the two different NTs depicted in Fig. 3. The abscissa is the y -axis of the two curves in Fig. 3. Clearly, the gray NT along the MEP to the dissociation following the direction of the y -axis crosses the BBP line at a lower value, it has a lower maximum of 76.1 force units with respect to the maximum of 108 force units of the other NT pictured in color blue that follows the $\mathbf{f}_{1,1}$ -direction. It shows (it is the proof for this model system) that an end-to-end pulling will need a stronger force for the dissociation of the AB bond than pulling along a single bond. It also shows that the simplified ansatz that the pulling direction is the 'reaction coordinate'²⁹ will generally be not correct.

An important tool of the data study from atomic force microscopy is the force-extension curve. The black curve in Fig. 4(a) only serves to invert to get the corresponding curve in panel (b), because the extension of the linear molecule is $R = x_0 + y$, thus only the y -axis is to move to the R -axis and $|\mathbf{g}| = F$ is fulfilled. The blue curve is still stretched in R -direction by the extension $R = x + y$ for the molecule. Note the concave finale at the BBP of the force-extension curves. It is due to the inversion of the convex maximum region of the gradient profile.

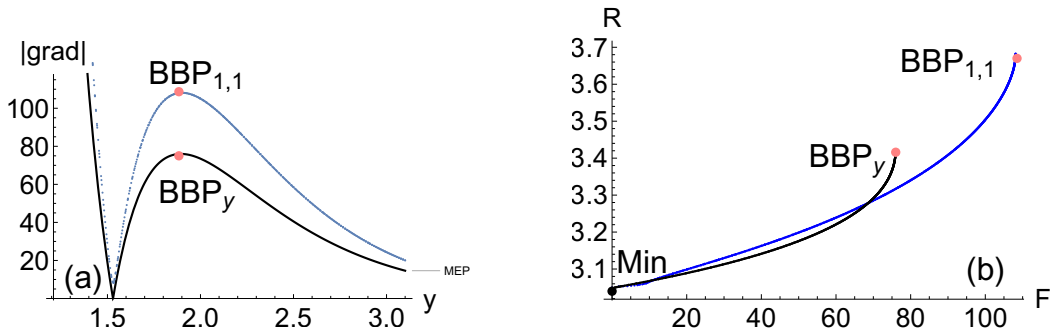


Figure 4: (a) The gradient norm over two Newton trajectories on the original 2D-Morse potential Eq.(6), compare a similar series of figures in Ref.⁵³ The black one is the gradient norm over the MEP in y -direction, the blue one over the $NT_{1,1}$ near the VRI point and then back to the y -valley. For comparison, the abscissa is the y -axis of Fig. 3. Note, the maximum over the blue gradient norm is at 108 units of derivation of Eq.(6). It is higher than the maximum over the NT along the MEP at 76.1 units. The MEP along the black curve goes through the optimal BBP. (b) Force-extension curves are shown for the two cases of panel (a). It is $F = |\mathbf{f}|$. For the black curve, it is the stretching degree of freedom $R = x_0 + y$, but for the blue one it is $R = x + y$.

The curves end at the BBPs because here, or usually before, the weakest bond breaks. The black curve gives the optimal amount for the breaking of the y -bond. For the blue curve we get a higher force: the additional energy is stored in a different degree of freedom. Under the break of the y -bond, this energy becomes free, in form of vibration of the remaining bond, or of heat dissipated into the environment.

3.2 Step two: pulling symmetrically into the BBP region of the ABC molecule

Applying the symmetric end-to-end pulling along the ABC linear symmetry corresponds to following the quasi-symmetric NT path for the FDSPs. If we apply a stronger symmetric force, $-73(1, 1)^T$, to the PES, we get the effective PES depicted in Fig. 5. The stationary points, minimum and SP_y , as well as maximum and SP_x , move together along the mentioned $NT_{1,1}$. The bowl of the minimum, as well as the summit of the maximum become flatter and flatter. In this case, starting from the minimum, one goes through the direction of the reaction valley parallel to the y -axis.

Now we imagine a force near, but below the critical force, \mathbf{f}_c , like in Fig. 5. Being in such effective minimums near the BBP enhances the reaction rate of a thermal escape; corresponding formula along special 1D potential curves are given elsewhere.⁴⁰

3.3 Step three: find the minimum of the symmetric force for the final BBP

Now we finish the pulling at the BBP point along the symmetric NT. This happens for the norm $|\mathbf{f}_c| = 76\sqrt{2} = 108$ units of the force, compare Fig. 4. We can divide this amount into

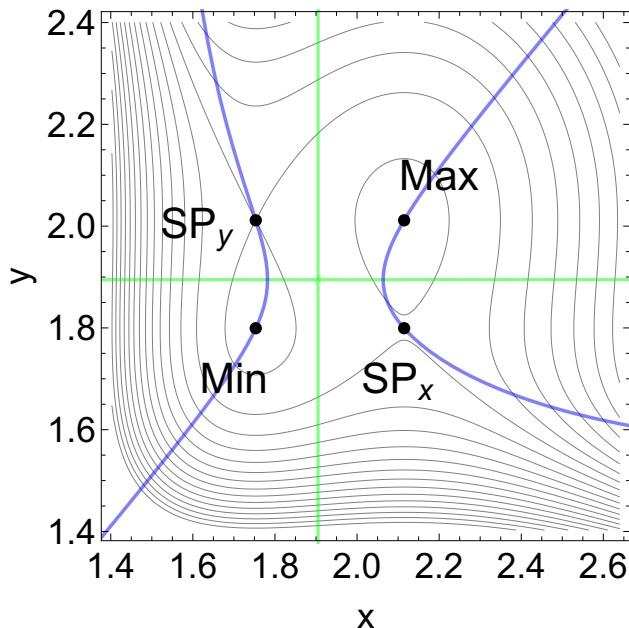


Figure 5: Effective 2D-Morse potential with $\mathbf{f} = 73(1, 1)^T$. The stationary points move together. The blue curve remains the NT to direction \mathbf{f} . The green lines are again the BBPs. The cross of the green lines is the VRI.

≈ 76 units for the y -bond, however, the remaining 32 units are stored in the x -bond. The final effective PES is given in Fig. 6. The former minimum, SPs and maximum disappear, they form two shoulders: one in the y -valley which is the final dissociation pathway, and one on the nearby ridge. The ridge also points into the y -direction and unites the former maximum and the SP_x .

The difference of the shoulders, Sh_y and Sh_x , is due to the asymmetry of the original Morse PES of Eq.(6). To reach the quasi symmetric singular NT to cross the VRI point, we have to use the direction $(1, 0.94)^T$. This is shown in Fig. 7 left panel (a) with the final amount of force from the former Fig. 6 with the factor 76. Such a complicated pulling direction can theoretically be imagined by an ABC molecule, if the central atom B is fixed, and if the two different amounts point along the bonds, x, y , of the atoms C and A. This amount is, however, not the BBP of this direction. We still have to add a little force up to a value of 81. The final effective PES is given in Fig. 7 right panel (b). The shoulder, Sh, has the form of a 'monkey-shoulder' of a threefold kind. A pulling into the direction would reach an equal probability for a dissociation of the molecule into three single atoms, A, B and C, along the diagonal part of the singular NT, or to the diatoms, AB or BC, if one follows the side branches after the bifurcation.

4 Case of a linear polymer chain

We treat a linear polymer chain in solution under the force of an ultrasound. The center of the chain may be the molecular part -ABBA- with similar Morse relations for (x, y) like in Eq.(6), compare Fig. 8. The scheme shows this linear part together with the two different

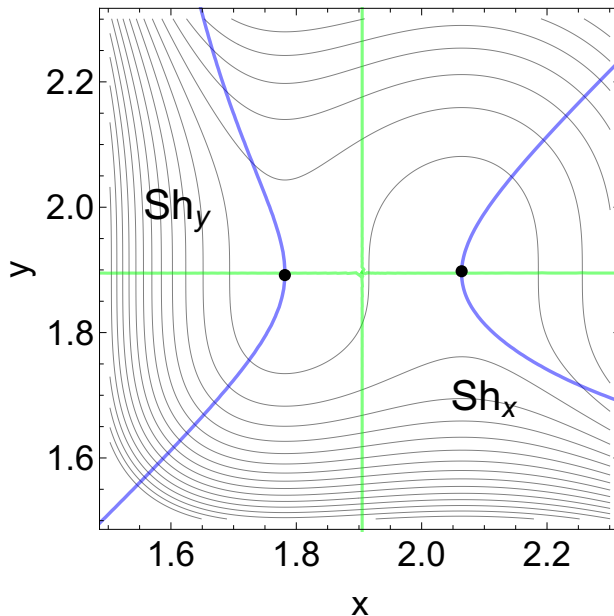


Figure 6: The final effective 2D-Morse potential with $\mathbf{f}_c = 76(1, 1)^T$ thus $F = 108$ units, the amount of force of the BBP along the blue NT to direction $(1, 1)^T$. The former stationary points disappear; their last emergence are the shoulders, Sh_y and Sh_x . The BBP of this pulling is the point Sh_y , the $BBP_{1,1}$. The green lines are the BBPs.

forces, \mathbf{f}_B for the BB-bond alone and \mathbf{f}_A at the two AB-bonds which apply to the corresponding bonds under a sonication. The initial and the end parts of the chain are symbolized by the symbols C_n . There are many experimental hints that the force distribution in the chain goes approximately with the square of the number of the bond in the chain,⁸³ up to the center. One assumes a mechanical cleavage due to cavitation events by collapsing microbubbles. The destructive force can be caused by ultrafast shear flow of the solvent.⁸⁴ Experiments have found that the rupture is near the midpoint of the chain.⁸⁵ In Fig. 9(a) it is assumed that the stronger B-B-bond breaks, along the x -axis, because it is in the center of the chain. Assuming for simplicity here number 3 for the first AB-bond and number 4 for the BB-bond, in the left half of a symmetric chain of 7 bonds, we get a relation of 9 : 16 for the forces along bonds y and x . The full force vector would point along direction $(1, 4, 9, 16, 9, 4, 1)^T$ in the coordinate space of all bonds, and should be still normalized to a unit vector by $2\sqrt{113}$. If we use a projection of the full PES of the chain into the plane of the x -bond and the one y -bond on the left hand side of Fig. 8, we can represent the pulling problem by a similar PES like in Fig. 2. The escape in the x -direction is enforced, however, the escape in the y -direction is inhibited by a relatively higher barrier.^{53,54,64} Now the NT which belongs to the pulling direction, \mathbf{f} , proceeds 'below' the VRI point, in the x -valley of the stronger bond. Since the other bonds in the chain are of similar strength then the crash by sonication of the chain will take place for the y -, the x -, or the other y -bond but mainly in the x -bond. The effective PES of a force with the given relation for the force direction is shown in Fig. 9(a).

It is well known that the incorporation of a single weaker bond within a polymer chain can alter the mechanochemical scission behavior⁸⁶ (specifically the selectivity of the pro-

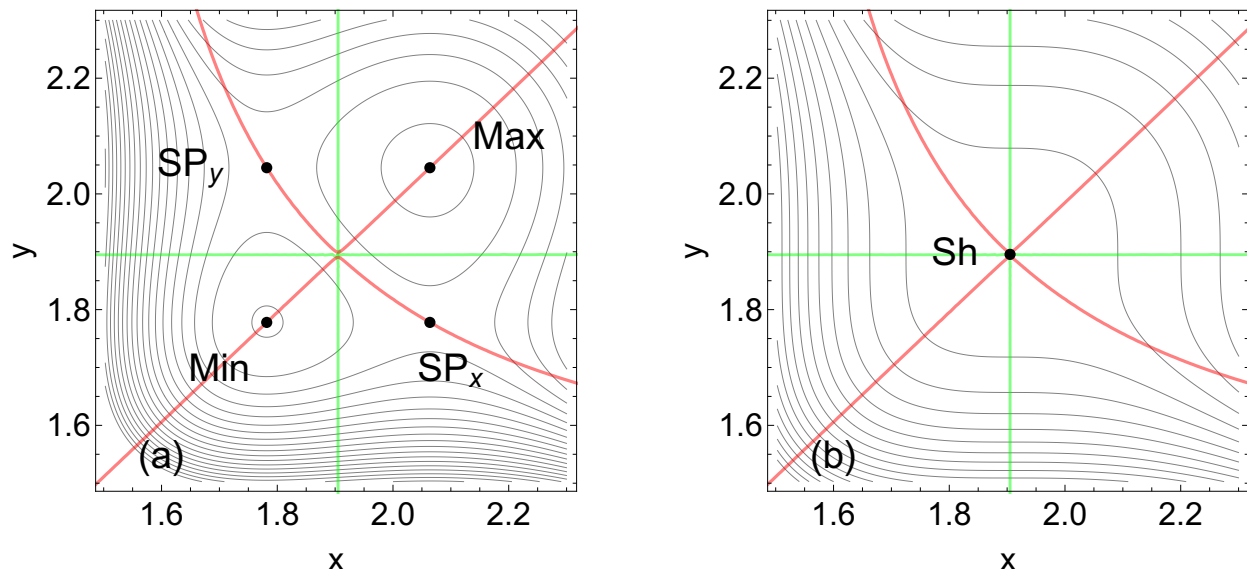


Figure 7: (a) Effective 2D-Morse potential with the force $\mathbf{f} = 76 (1, 0.94)^T$, the amount of force of the BBP along the blue NT to direction $(1, 1)^T$ of Fig. 6. The current singular NT is red. It directly crosses the VRI point. (b) Final effective 2D-Morse potential with $\mathbf{f} = 81 (1, 0.94)^T$. It is the final amount of force for the (maximal) BBP being the VRI point of the PES. The former stationary points disappear; their last emergence is the shoulder, $\text{Sh} = \text{VRI} = \text{BBP}_{\max}$.

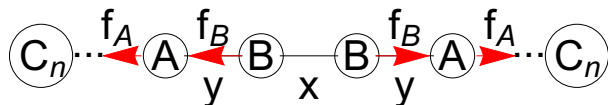


Figure 8: A schematic part of the center -ABBA- of a polymer chain. The arrows \mathbf{f}_A and \mathbf{f}_B are the pulling forces originating in a sonication experiment with a different magnitude.

cess). Examples are, e.g., due to Sijbesma et al.⁸⁷ which show that the limit below which a mechanochemical chain scission of a polymer is not possible, can be reduced when a covalent C-C bond near the center of the polymer backbone is replaced by a weak metal-ligand coordination bond. The effect of this metal-ligand can be well rationalized theoretically. We note that the precise location of the mechanochemical scission could be programmed to some extent by placing the mechanophore in an 'off-center' position along the polymer chain as discussed in Refs.^{85,88} Even though this bond does not experience the highest force, its lower strength still ensures selective scission. We demonstrate this by a further example: we change the left y -bond in the toy polymer, Fig. 8, into a weaker z -bond with

$$M_3(z) = D_3 (1 - \exp[-\beta_3(z - z_0)])^2 \quad (8)$$

$$V_3(x, z) = M_1(x) + M_3(z) \quad (9)$$

with $M_1(x)$ given above in Eq.(6) and the constants are now:

$$D_1 = 90, D_3 = 45, \beta_1 = 1.8, \beta_3 = 1.95, x_0 = 1.52, z_0 = 1.53.$$

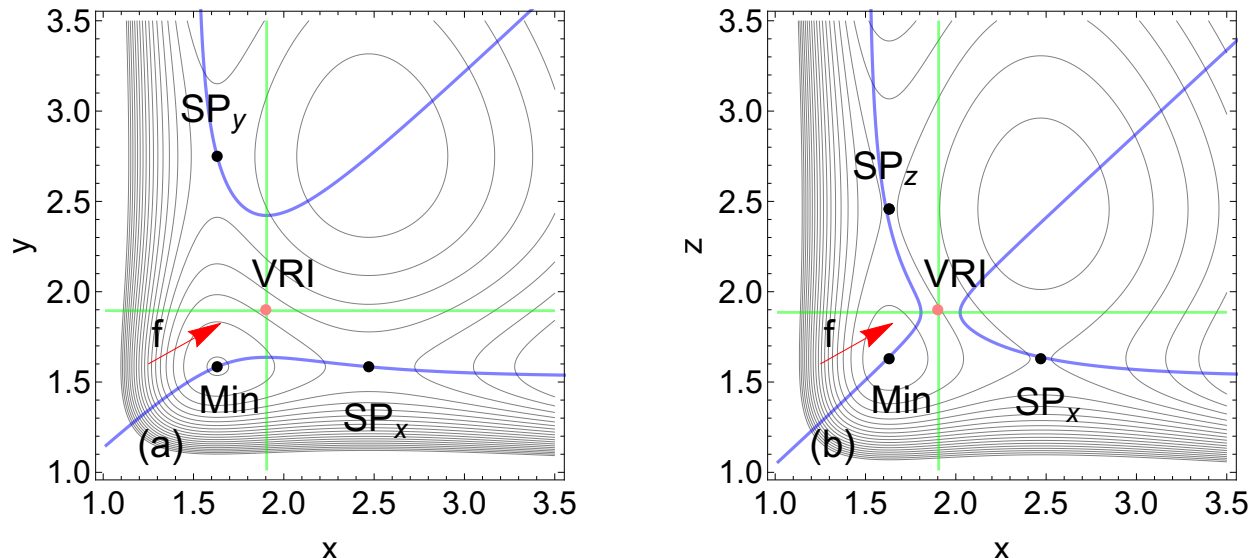


Figure 9: (a) Effective PES projection of the chain of Fig. 8 with Morse constants of Eq.(6) and Fig. 1. The new NT (blue) points in the direction $(16, 9)^T / \sqrt{337}$. The direction of \mathbf{f} is the red arrow. The pulling force is $-3(16, 9)^T$ for the effective PES in Eq.(1). The amount is near Fig. 3, however the force points in a different direction. It changes the lowest dissociation path into the x -direction 'below' the VRI point. The green lines are the BBPs. (b) Effective PES of the new surface V_3 of Eq.(9) with a quite weaker bond in z -direction but the same drag force like in panel (a). Now the NT from the minimum turns into z -direction.

For this new PES the NT along the same force $-3(16, 9)^T$ turns back into the z -direction, 'above' the VRI point, and the z -bond will break first under this force, see Fig. 9(b).

It is thus to conclude that if the bond of the mechanophore is weak enough then the scission of the polymer can take place before the center of the chain. The balance between 'weakness' of the mechanophore and concentration of the force to the center is decided by the VRI point of the PES. This highlights the importance of the VRI points and the importance of their location.^{89,90}

If the polymer is not linear then the competition entry of the different bonds become quite more complicated,⁷⁸ compare also the next Section 5.

5 Model PES for a pulling of a bent ABA molecule with C_{2h} symmetry

5.1 The model

We will now treat a triatomic molecule with an equilibrium angle, say 60° . Fig. 10 shows the geometry, and an assumed pulling direction, $\mathbf{f}_{x,\alpha}$. The force, $\mathbf{f}_{x,\alpha}$, should pull in the fixed 'horizontal' direction in Fig. 10. The PES may be a Morse curve for the x -distortion

$$M_1(x) = D_1(1 - \exp[-\beta_1(x - x_0)])^2$$

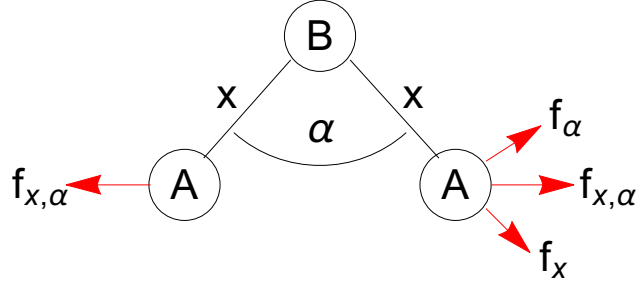


Figure 10: A schematic bent 3-atomic molecule ABA. The atoms are connected by Morse potentials. The arrow, $\mathbf{f}_{x,\alpha}$, depicts the pulling force: its action for the internal coordinates, $(x, \alpha/2)$, changes with the opening of the bending.

with $D_1 = 90$, $\beta_1 = 1.8$, $x_0 = 1.52$, and for the angle

$$W_{ABA}(\alpha) = D_\alpha \sin\left(\frac{3}{4}(\alpha - \pi/3)\right)^2 \quad \text{for } \pi/3 \leq \alpha \leq \pi . \quad (10)$$

Because the potential energy of an angle is usually quite lower than the energy of the bonds,^{91,92} we assume for the force constant $D_\alpha = 20$. The $\alpha_0 = \pi/3$ is used for the equilibrium value. The PES is

$$V(x, \alpha) = 2 M_1(x) + W_{ABA}(\alpha) . \quad (11)$$

Now, the forces, $(\mathbf{f}_x, \mathbf{f}_\alpha)^T$, in direction to (x, α) are changed with a changed angle: the relation is given by a force parallelogram, compare Fig. 10, where the applied $\mathbf{f}_{x,\alpha}$ splits into $F(\sin(\alpha/2), \cos(\alpha/2))^T$ and an effective PES is

$$V_{eff}(x, \alpha) = V(x, \alpha) - F\left(\sin\frac{\alpha}{2}, \cos\frac{\alpha}{2}\right)(x, \alpha)^T . \quad (12)$$

Such a force is not constant for changing angles α , so there follows that we cannot apply the theory of NTs. However, we can calculate the stationary points of the effective PES directly. It is similar to the COGEF method (CONstrained Geometries simulate External Force)⁹³ where two anchor atoms are elongated in small steps, and the molecular geometry is optimized at each step. The calculation is done here for the representation of Eq.12. The curve of the blue points, $\text{Sol}_{x,\alpha}$, in Figs. 11-14 are constructed by such solutions. Note that applying the tensile force alone along f_x or f_α would generate a translation motion of the whole molecule. This is not treated here because we only use the internal coordinates x, α . Fig. 11(a) shows the original PES of Eq.(11). Included are the two direct NTs (gray), NT_x and NT_α , along the valleys, and the singular NT (red) through the VRI point for comparison. Fig.11(b) shows the effective PES with $F = 10$ units in Eq.(12). $\text{Sol}_{x,\alpha}$ depicts a set of force-displaced stationary points for a different amount, F , of the force vector in Eq.(12). The set is overlayed over the PESes in Figs. 11(a,b), Figs. 12(a,b) and Fig. 14(a). The set of solutions shows that the force is not able to turn the bent molecule into a linear molecule, however, the angle stabilizes near the α -value of the VRI point, it is so to say near an α_{limit} value. (It is in contrast to an assumption in Ref.²⁷) Here the bond stretching goes on up to the BBP point, see Fig. 12(b). The former BBP lines with Eq.(5) now change

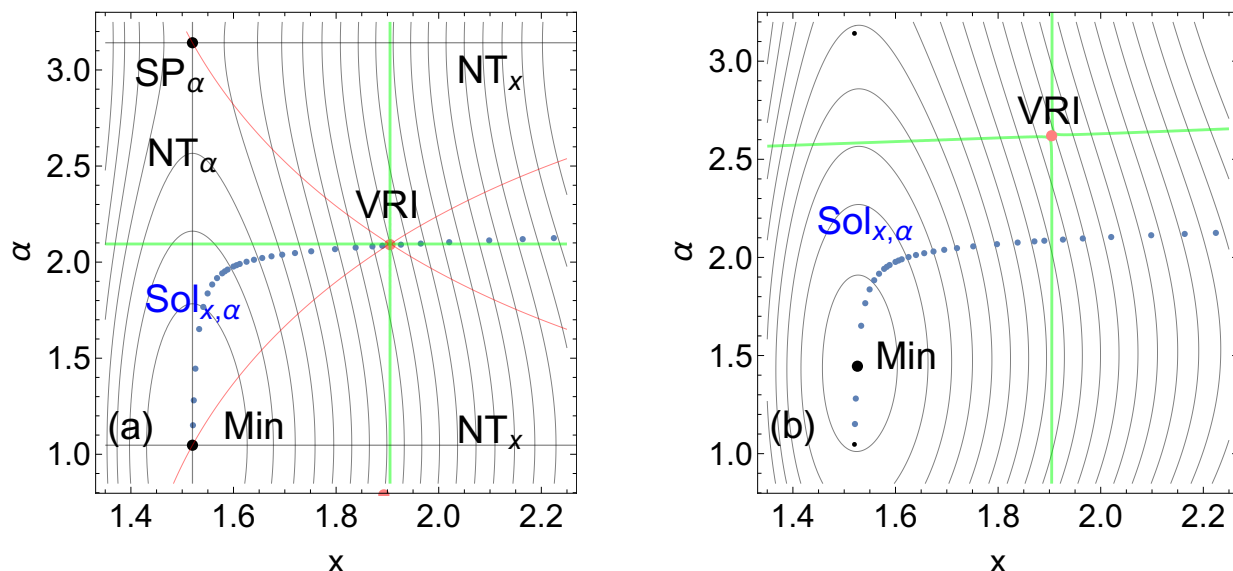


Figure 11: (a) 2D surface of Eq.(11) with Morse potential for x and angle-potential for α . The blue points are the solution points for zeros of the effective PESes in the variable pulling direction for increasing F . The singular NT through the VRI point is red. It is given for comparison. In small gray are shown the direct NTs in x - and α -directions. (b) Effective PES for $F = 10$ units of PES (12). The minimum has moved uphill, as well as the SP_α . Now the Hessian is not constant, so the VRI point has also moved.

under the pulling for every effective PES, because the pulling direction is not constant. It can be observed in Fig. 11(b) where the effective VRI point has also moved.

Fig. 12 shows two further effective PESes. One for $F = 100$ units in panel (a), and the final effective PES for $F = 187.44$ units in panel (b). For higher forces than the $F = 100$ units in case (a) the change of the molecule is mainly in the x -elongation. The force $F = 187.44$ is the final amount of force for the BBP of $\mathbf{f}_{x,\alpha}$. The BBP is the former VRI point of the PES (red). The former stationary points disappear; their last emergence is at the one shoulder. Because the molecule is symmetric, there both x -bonds break (theoretically) at the same point.

If we compare this example, the molecule of Fig. 10, with the linear case, Fig. 1(a), then we see that a curve of FDSPs also emerges here, the points of $Sol_{x,\alpha}$. Though this curve is not an NT, along its pathway the effective PESes have the same qualitative behavior like the effective PESes along an NT: the way finally ends in a shoulder at the BBP.

5.2 Force-extension curve

We still calculate the representation of an extension of the ABA molecule under the force, $\mathbf{f}_{x,\alpha}$, see Fig. 10. The distance R between the two A-atoms is $R = x \sqrt{2(1 - \cos\alpha)}$ where we have used the cosine formula in the triangle with equal sides, x . The total length, L , of both bonds is $2x$. Fig. 13(a) shows the relation of the total length L to the end-to-end extension R of the points of the calculated $Sol_{x,\alpha}$ curve between minimum and BBP, the

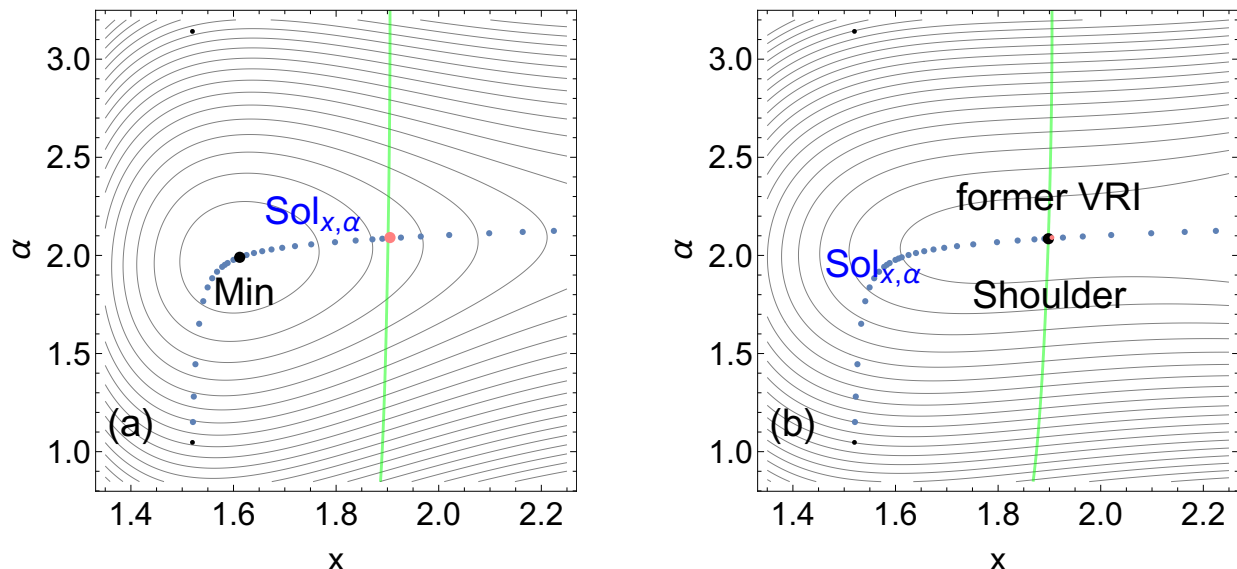


Figure 12: (a) Effective PES for $F = 100$ units of PES (12). The minimum has moved further uphill. In the shown region, only the BBP curve (green) in the x -direction is present. The blue points on the right hand side of the BBP line are saddle points, SP_x , which move to the left with increasing F . (b) Final effective PES for $F = 187.44$ units of PES (12). The former minimum and the SP_x coalesce in a shoulder, interestingly exactly at the VRI point of the original PES (but that is an artifact, see text).

shoulder in Fig. 12(a). At the beginning, for small forces, mainly the angle is flattened. It makes a strong increase of R . Later the angle reaches its quasi-limit, and the relation of L to R quasi goes linear. Panel 13(b) shows the corresponding force-extension curve for the bent molecule. Because Eq.(12) is a 'nonlinear' model for a pulling, the stationary points of the corresponding effective PES go with the derivations for $\nabla_{(x,\alpha)}^T V(x, \alpha) = (V_x, V_\alpha)^T$

$$V_x = F \sin \frac{\alpha}{2} \quad (13)$$

$$V_\alpha = F \left(\frac{x}{2} \cos \frac{\alpha}{2} - \frac{\alpha}{2} \sin \frac{\alpha}{2} + \cos \frac{\alpha}{2} \right). \quad (14)$$

Thus the amount F of the force has to be higher, usually, than the $|\nabla V(x, \alpha)|$ of the PES. But at the BBP the norm $|\nabla V(x, \alpha)|$ has also its maximum on the $Sol_{x,\alpha}$ curve because there the angle, $\alpha \approx \alpha_{limit}$, is nearly constant.

We can compare the curve of Fig. 13(b) with the similar curves of Fig. 4(b). For a single bond to break, the black curve in Fig. 4(b), the critical force, \mathbf{f}_c , has to come near 76 units. For the end-to-end drag force of the linear triatomic we need 32 units more, the blue curve in Fig. 4(b). In the case of the bent ABA molecule with its $x - \alpha - x$ potential we need for \mathbf{f}_c the value of 187 units. The amount includes the somewhat flattened angle α and the stretching of the two equal bonds, x . Note that the gradient of the original PES at the BBP has only a norm of 162.5 units, thus it is $\approx 13\%$ lower than F . That Eq.(2) does not fully hold for some pulling experiments was already stated in Ref.⁹⁴ We find here in the example

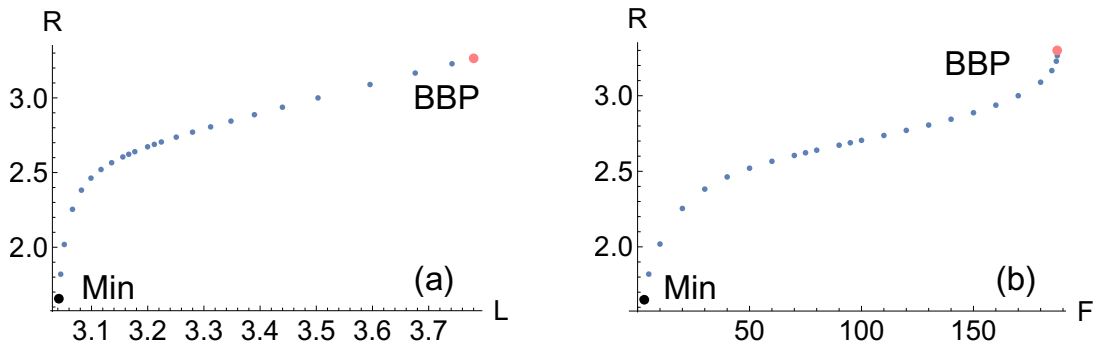


Figure 13: (a) Total bond length to extension for the points of $\text{Sol}_{x,\alpha}$ of the ABA molecule. (b) Force-extension curve for the ABA molecule, see text. The concave arc before the BBP represents the flat shoulder of the 'last' effective PES, see Fig. 12(b). Here only a small increase of the force, F , causes still a large increase of the extension, R .

the reason in the nonlinearity of the ansatz Eq.(12).

There is a further difference between the force-extension curves of Fig. 4(b) and Fig. 13(b). In Fig. 4(b) we have a linear increase up to the final concave arc before the BBP. In Fig. 13(b) we find two quasi linear parts before the final concave arc of the BBP. The reason is that in the linear molecule only bonds are stretched, however, in the bent molecule first the angle is flattened, and later the bonds are stretched. This causes two different parts of the force-extension curve. It is a hint to the higher-dimensional character of the problem – though we have an 1D curve of FDSPs.

If one imagines not only two bonds, but a longer nonlinear polymer chain with many bonds and angles, then the corresponding force-extension curve for the so-called 'wormlike chain' will emerge with added extensions and added parts of the force stored in the many bonds and angles. However, we guess that the qualitative shape of the curve will hold this form of our simple three-atomic molecule ABA. For every kind of bonds we will find a nearly linear part of the force-extension curve, connected by a convex arc to the next kind of bonds. One can compare it to the result of former derivations.^{94,95}

Of course, for much bigger molecules like peptides, the different kind of forces may overlap, like the loss of configurational entropy and the relaxation of tertiary structures,⁹⁶ coil-stretch transitions,⁹⁷ loop-stretch transition,⁹⁸ H-bond breaks, and so on.

In Fig. 13(a) we see that $R < L$ always holds because the angle is limited to its quasi final value for higher forces. That will also hold for longer chains. By the way, the celebrated formula of Marko and Siggia^{99,100} for the entropic force extension in wormlike chains is

$$F = \frac{k_B T}{A} \left(\frac{R}{L} + \frac{1}{4(1 - R/L)^2} - \frac{1}{4} \right)$$

where A is a bending stiffness parameter (also named persistence) and $k_B T$ is the thermal energy with Boltzmann constant and absolute temperature. The region for a limit $R \rightarrow L$ is excluded here by the divergence of the expression, it becomes unphysical. Any kind of 'cut-off-force' as the force which is required to stretch a molecular chain with length R into

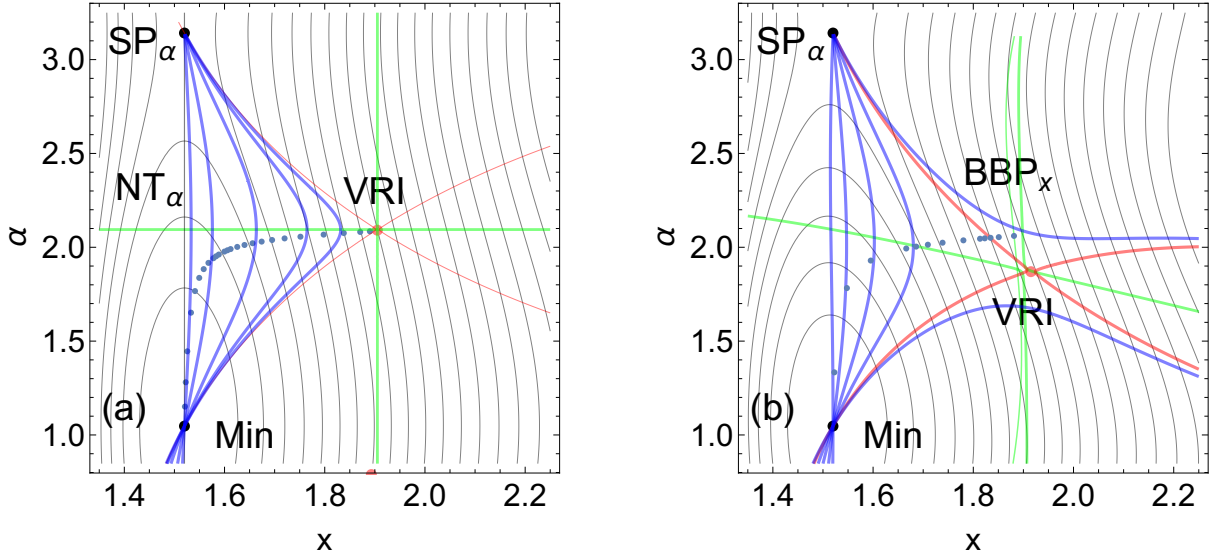


Figure 14: (a) The original PES of Fig. 11(a) with regular NTs of the minimum-to- SP_α -family. The thin gray NT is the direct NT in the valley up to SP_α . The other regular NTs (blue) cross the $Sol_{x,\alpha}$ curve in the minimum bowl before the crossing of the singular NT at the VRI point. The corresponding gradient directions there give the constant directions of the NTs. They are shown in Table 1. The red curve is the singular NT which is the border of the given family of NTs. The BBP curves (green) are also presented. (b) A PES where the two dimensions are slightly coupled, see Eq.(15). The green lines are the $Det(\mathbf{H}) = 0$ lines, the two thick curves are those of the original PES, but the thin green line is the same for the effective surface of the VRI point. Blue points are the solution points of the curve $Sol_{x,\alpha}$ which leads correctly up to the green line, the BBP_x . Blue curves are regular NTs.

its total contour length L^{95} seems to be a not correct ansatz.

In all known experiments, to the best of our knowledge, there is missing the final concave arc of the force-extension curve before the BBP.^{62,96,99,101–104} It demonstrates that the flat region of the effective PES before the BBP, like in Fig. 5, 7(a) or 12(a), is not the region of stable molecular states. If the external force decreases the barrier to a certain amount then the crossing of the region takes place immediately. This kinetic fact is due to finite temperature effects. The measured force-extension curves finish before the final concave arc before the BBP. They represent only a certain part of the FDSPs curve.

5.3 A coupled PES model

It seems strange that the pathway of the force-displaced stationary points, $Sol_{x,\alpha}$, crosses the BBP_x curve at the VRI point of the original PES without load. However, the fact is a coincidence due to the very simple toy PES with a decoupled ansatz of both dimensions, x, α . While here the forces f_x and f_α are dependent on α , we cannot apply the NT-theory. But to a certain degree, it comes in by a loophole. We have for every fixed point (x, α) a fixed force (f_x, f_α) . If we assume the direction of this force fixed, then we can take an NT through the corresponding effective stationary point of the $Sol_{x,\alpha}$ curve, but now taken on

the original PES. For all points of the curve we have such an NT. They form the family of NTs which connect the minimum and the SP_α . Note that the border of the family is the singular NT (red in Fig. 11(a)). The force (f_x, f_α) turns from a more or less α -direction at the beginning into x -direction for a higher α value, see Table 1 and Fig. 14(a). This happens at the crossing of the $Sol_{x,\alpha}$ curve with the BBP curve. After this crossing the corresponding $Sol_{x,\alpha}$ points belong to another family of NTs which does not make its way to the SP_α . Thus the singular NT of the original PES marks the border of a qualitative transition of the used force direction.

Table 1: Directions of the NTs of Fig. 14(a) for some points of the $Sol_{x,\alpha}$ curve

x	α	
0.0	1.0	NT_α
0.7071	0.7071	Start NT
0.9659	0.2588	
0.9914	0.1305	
0.9949	0.1004	
0.9956	0.0940	
0.9957	0.0922	Sing. NT

In Fig. 14(b) we test a slightly coupled PES with the additional function

$$Coupling(x, \alpha) = 11 \sin\left(\frac{3}{4}\left(\frac{x}{x_0}\alpha - \alpha_0\right)\right)^2 \quad (15)$$

added to the original PES of Eq.(11) in Fig. 11(a). It may mirror the influence of the bond length, x , on the angle potential. Countour curves belonging to the PES in Fig. 14(b) correspond to the equation (Eq.(11)+Eq.(15)). There are the blue regular NTs, the red singular NT, and the two green BBP curves which also include the VRI point. Under a force like in Eq.(12), now, the BBP_x line also changes slightly with different effective forces. In Fig. 14(b) we have added a thin green line which is the BBP line for the effective force at the singular NT. The points of the curve $Sol_{x,\alpha}$ for increasing values of F now cross the singular NT anywhere before the BBP_x curve. Clearly the theory of NTs with a constant direction of the pulling force is not applicable here. The curve of the FDSPs, $Sol_{x,\alpha}$, finally tends into the x -direction, however, it crosses the singular NT between VRI point and SP_α , and not 'below' the VRI point, compare Figs.9(a,b).

Note that coupled degrees of freedom of the PES, but under a fixed force direction, are treated elsewhere.^{49,53,54,63,66}

6 Case of a planar 4-atomic ABBA molecule with C_{2h} symmetry

We treat the case of a four-atomic chain with an ansatz of three Morse-potentials for the bonds. In three dimensions, we still can imagine the VRI point.¹⁰⁵ If one of the three bonds is broken, the other minimums remain after the bifurcation.²²

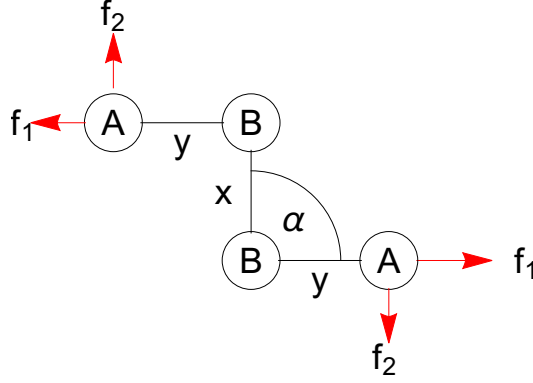


Figure 15: A schematic 4-atomic molecule ABBA. The atoms are connected by Morse potentials. The arrows, \mathbf{f}_1 or \mathbf{f}_2 , depict the pulling forces for two different end-to-end actions.

In Fig. 15 we assume two different Morse potentials between the two AB-bonds and the one BB-part, and two angles α between the two B-atoms and the outer A-atoms. We further assume a flat molecule in a plane. The potential of the angle, α , may be a simple trigonometric function. For the pulling we need it between $\alpha = 90^\circ$ and 180° . The contribution of the energy potential from the angle B-B-A is given by

$$W_{BBA}(\alpha) = D_3 \sin(\alpha - \pi/2)^2. \quad (16)$$

Because the potential energy of the angles is usually quite lower than that of the bonds, we assume $D_3 = 20$. The full expression of the PES for the ABBA molecular system is assumed to be

$$V(x, y, \alpha) = 2 M_{AB}(y) + M_{BB}(x) + 2 W_{BBA}(\alpha). \quad (17)$$

Here $M_{BB}(x)$ and $M_{AB}(y)$ correspond to the functions $M_1(x)$ and $M_2(y)$ of Eq.(6), respectively, while $W_{BBA}(\alpha)$ is given in Eq.(16). We note that if any external, end-to-end force is applied to the molecule, see Fig. 15, it also pulls on the angles. If we approximate that the change of the angles is independent of the stretchings of the bonds then it does not make a difference if one uses either \mathbf{f}_1 or \mathbf{f}_2 of Fig. 15, or any direction in between. For \mathbf{f}_1 , the transmission of the force goes over the bonds y to the angles, but for \mathbf{f}_2 , the force acts directly to the angles. If we assume C_{2h} symmetry for the ABBA system both forces \mathbf{f}_1 and \mathbf{f}_2 modify the two α angles. Note that the forces depicted in Fig. 15 will generate a torque on the molecule. That is the reason why we assume a force of 45° between \mathbf{f}_1 and \mathbf{f}_2 , see Fig. 16. With the result of the previous section we can assume that the outer force flattens the angles α up to a quasi final limit value, α_{limit} , and then a further amount to \mathbf{f}_{limit} of the force continues to elongate the bonds only. The center of mass of the molecule is in the middle of the B-B-bond. The molecular plane, constituted by the four atoms ABBA, is normally the binary axis C_2 which is an element of the C_{2h} point group of symmetry.

We now treat larger forces than \mathbf{f}_{limit} . We are interested in the relation of the two forces, \mathbf{f}_y and \mathbf{f}_x , see Fig. 16. By the force parallelogram, drawn schematically on the right hand side of the skew molecule under the force, see Fig. 16, we can calculate the single forces on the bonds. With the three angles α at B, β at $x/2$, and γ at A, we get by the sine theorem

$$\mathbf{f}_x = \mathbf{f}_{limit} \frac{\sin(\gamma)}{\sin(\alpha)}, \quad \mathbf{f}_y = \mathbf{f}_{limit} \frac{\sin(\beta)}{\sin(\alpha)}. \quad (18)$$

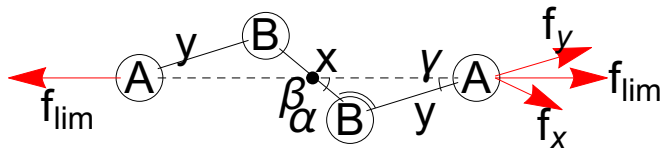


Figure 16: The 4-atomic molecule ABBA under a stronger force behind \mathbf{f}_{lim} . The arrows \mathbf{f}_y and \mathbf{f}_x are the forces for the two bonds.

In the triangle of the right half molecule we have the sides y and $x/2$. If we assume that x and y are nearly of equal length, then the angles β and γ are in the relation

$$\sin(\gamma) \approx \frac{1}{2}\sin(\beta) .$$

If we further assume that β and γ are small angles then the forces also go approximately with 1:2. But in the right triangle we have only treated the half bond $x/2$, so, it finally comes out that nearly equal forces act to the three bonds in the ABBA molecule, for the elongation of the bonds.

Finally the VRI points between the different stretching directions decide which bond breaks. For an end-to-end pulling we find that the weakest bond breaks. If we use the values of Eq.(6) then again the two weaker y -bonds break first but the stronger x -bond survives. Of course, which of the two equal y -bonds breaks first depends on the thermal noise in reality and may also depend on non equilibrium effects which may be described by a Franck-Condon theory of mechanochemistry.¹⁰⁶ The effects of thermal fluctuations have already been demonstrated to play a key role in mechanochemistry.⁶⁸ As a real chemical example we have the flattening of the -O-Si-O- bond angles in siloxanes, see e.g.^{107,108}

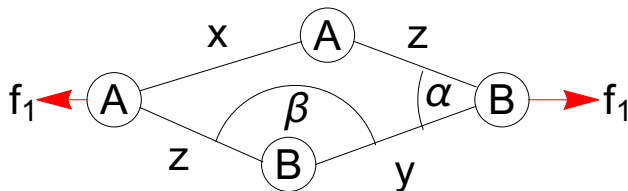


Figure 17: A schematic ring molecule AABB. The arrow \mathbf{f}_1 is the pulling force for an end-to-end action with the direction along the larger diagonal of the molecule.

7 Case of a planar 4-ring AABB molecular model with diagonal pulling

In Fig. 17 we schematically depict a 4-ring. The coordinates x, y depict the bonds x between atoms A-A and y between atoms B-B, and now here z depicts the bonds between A-B atoms correspondingly. Two next internal coordinates, β , are the angles between the bonds which are stretched, B-B-A, for the three lower atoms in Fig. 17, and between A-A-B for the three upper atoms. Now α are the angles between the bonds which are compressed, A-B-B, for

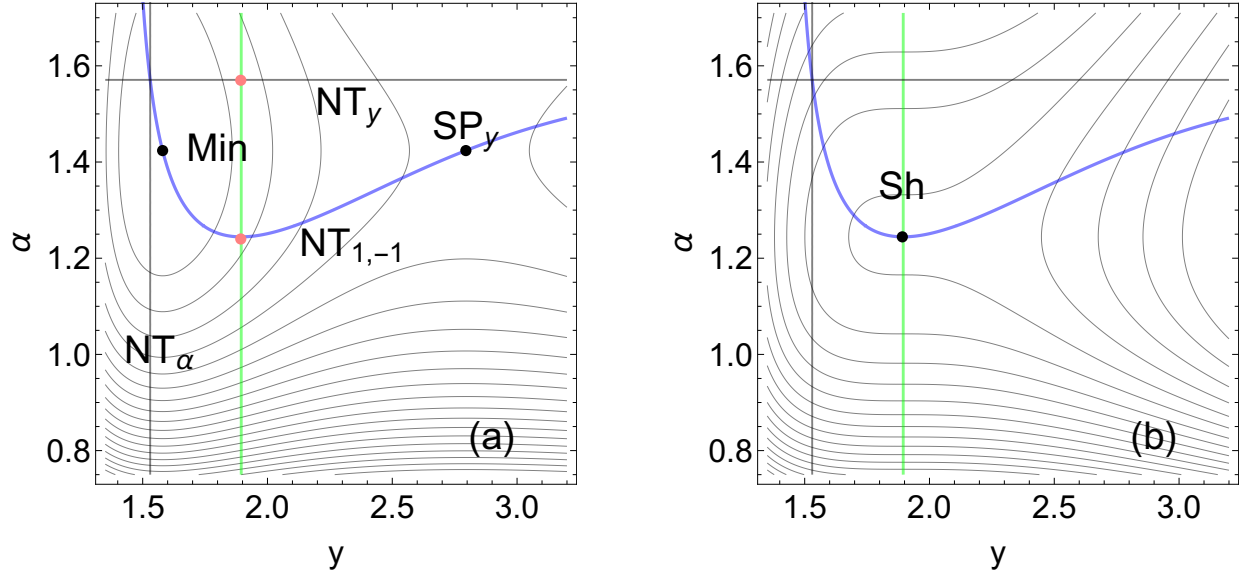


Figure 18: Effective PES $V_{eff}(x, y, z, \alpha, \beta)$ for the force \mathbf{f}_1 of Fig. 17 in a projected section in the (y, α) -plane. In color gray are depicted the NTs in y - and α -direction of the original PES. Two cases of the amount of (a) $\mathbf{f}_1 = 25(1, -1)^T$ and (b) $\mathbf{f}_1 = 76(1, -1)^T$. The y -axis is the bond y and α is the compressed angle under the force with potential Eq.(21). The blue curve is the NT to direction \mathbf{f}_1 . The green line depicts the BBPs of the y -stretch. A VRI is missing here. The case (b) is the final force for the opening of the y -bond where Sh is the shoulder.

the three right atoms, and between B-A-A for the left three atoms, under the force \mathbf{f}_1 . With the results of Sections 5 and 6 we can assume that \mathbf{f}_1 is large enough to flatten the angles β nearly to its quasi limit. Then the direction of \mathbf{f}_1 in the remaining coordinate space of $(x, y, z, z, \alpha, \alpha)$ can be simplified to the direction vector $\mathbf{l}_1 = \frac{1}{\sqrt{6}}(1, 1, 1, 1, -1, -1)^T$.

We make the assumption that there is a nearly infinite force in the molecule to avoid a total compression of the angles α , thus we can assume further potential functions for $0 < \alpha \leq \pi/2$, $\pi/2 \leq \beta \leq \pi$

$$\begin{aligned} W_{BBA}(\beta) &= D_{BBA} \sin(\beta - \pi/2)^2, \\ W_{ABB}(\alpha) &= D_{ABB} (\pi/(2\alpha) - 1)^2 \end{aligned} \quad (19)$$

with $\alpha + \beta = \pi$, thus the β -function is flat, but the α -function becomes strong. We use a 'reflective' boundary for the energy function to prevent particle overlapping. The additional bond energy is

$$M_{AB}(z) = D_{AB}(1 - \exp[-\beta_3(z - z_0)])^2. \quad (20)$$

Note that this z -part is different to the z used in Section 4. We use the full PES of the ring molecule to be

$$V(x, y, z, \alpha, \beta) = M_{AA}(x) + M_{BB}(y) + 2M_{AB}(z) + 2W_{BBA}(\beta) + 2W_{ABB}(\alpha) \quad (21)$$

where $M_{AA}(x)$ and $M_{BB}(y)$ correspond to the functions $M_1(x)$ and $M_2(y)$ of Eq.(6), respectively. The function $M_{AB}(z)$ is that given in Eq.(20), and $W_{BBA}(\beta)$ and $W_{ABB}(\alpha)$ are

defined in Eqs.(19). Finally, the used constants are
 $D_1 = 90, D_2 = 80, D_{AB} = 100, D_{BBA} = 20, D_{ABB} = 120,$
 $\beta_1 = 1.8, \beta_2 = 1.9, \beta_3 = 2.0, x_0 = 1.52, y_0 = 1.53, z_0 = 1.5,$
 $\alpha_0 = \pi/2, \beta_0 = \pi/2.$

By our simplified ansatz of a nearly decoupled PES, we get again straight lines for the BBP curves in all coordinates, except for the angles α where no BBP exists under the ansatz of Eq.(19). With the given constants we further assume that the y -bond is the weakest bond. All the bonds are in relation like in the former Sections. Of interest is still a 2D projection of the full PES into the (y,α) -plane. The force \mathbf{f}_1 points into the plane of the projection into direction (1,-1). In Fig. 18(a) the line of BBPs (green) and three NTs is shown. The two gray lines are the NTs along the axes directions (1,0) and (0,-1). Because the potential energy for the (y,α) -coordinates is not coupled, these NTs are again straight lines. The blue curve is the NT to the direction \mathbf{f}_1 projected into the plane of interest. For decreasing α no SP exists. In contrast, the PES mountains tend to a quasi infinite slope. Consequently there does not emerge a line of BBPs in the decreasing α -direction. Only the BBP-line in y -direction is present. There does not exist a VRI point either.

Fig. 18(a) already shows an effective PES for $\mathbf{f}_1=25(1,-1)^T$. The minimum of this PES is already slightly destabilized, and an SP_y has emerged. Both stationary points are on the $NT_{1,-1}$ of the pulling direction, the curve of FDSPs. Fig. 18(b) is the final case at the BBP where the $NT_{1,-1}$ crosses the green line of the BBPs. The NT describes the movement of the two stationary points, minimum and SP_y . For a force with the norm $76\sqrt{2}$ the effective minimum and the effective SP_y coalesce and form a shoulder. Before the y -bond finally breaks. However, as can be well observed in the panel (b), a corresponding amount of “ α ”-force is absorbed: the shoulder is moved to an α value of $1.3rad$, at 75° , against $\alpha_0 = \pi/2rad$, at 90° . We need all the other parts of force which are absorbed by the other bonds for a bond breaking of the y -bond along force \mathbf{f}_1 .

By the way, the effect of a partially absorbed force is an old known effect: in an unfolding experiment of an RNA hairpin attached by handles of long semi flexible polymer chains, the value of the unfolding force increases as the length of the handles increases.⁷³ (Because the handles also absorb force.) For the opening of a ring as well, the force found was quite larger than the force for the breaking of the corresponding bond.¹⁰⁹

8 Case of a planar 4-ring AABB molecular model with pulling along a bond

The situation changes for another pulling force \mathbf{f}_2 along the y -bond only, see Fig. 19, also compare the ring opening in cyclobutane studied in a seminal paper,⁴³ as well as the ring opening in trans-3,4-dimethylbutene.⁴⁷ The two z -bonds, as well as the x -bond, are only spectators in this pulling. However, the two angles opposite α and β , at the two A-atoms, form a sum, $\alpha + \beta$, now playing the role of angle α in Section 5 for the opening of a bent triatomic molecule. Thus we will find a qualitative picture like in Section 5. The sum of angles, $\alpha + \beta$, may develop a potential energy under this pulling. But for an enhancement of the y -bond, and its final breaking, the angles at the two A atoms will finally get a quasi limit.

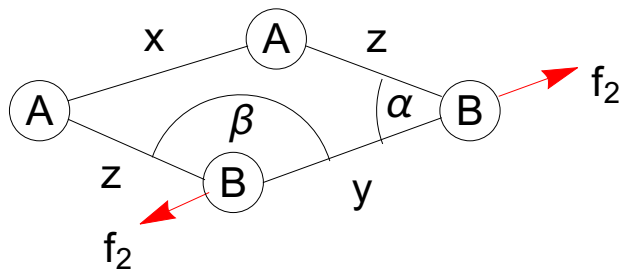


Figure 19: A schematic ring molecule AABB. The arrow \mathbf{f}_2 is the pulling force with the direction along the y -bond.

As expected, the pulling along a single bond in a ring molecule should exactly break this bond. However, the included angles being contrary to the bond also absorb a part of the energy. Here, the rupture of the y -bond will take place.

Beginning with the examples of Sections 7 and 8, one can also discuss the possibility of a 'rebinding', at a certain mild force, \mathbf{f} , after the 'unbinding' of the weakest bond.^{62,110} We do this in the next section.

9 Model for the unfolding of a hairpin

We still extend the former example to a toy 4-base pair hairpin, see Fig. 20, under the unfolding force, \mathbf{f} . Recently, real molecular examples were calculated, of a rubredoxin metalloprotein including some β -strands,⁷⁴ as well as the unzipping of a β -cyclodextrin with a pair of hairpins.¹⁴

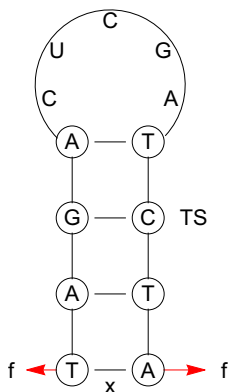


Figure 20: A schematic 4-base pair hairpin. The arrows \mathbf{f} are the drag force with direction along the elongation of the extension, x , of the $T - A$ base pair.

To simulate the unfolding we choose a simplified PES with the help function¹¹¹

$$de(x, y, x_0, y_0, e_x, e_y) = \text{Exp}(-e_x^2 (x - x_0)^2 - e_y^2 (y - y_0)^2) \quad (22)$$

to build the model PES

$$V_H(x, y) = (x - 2.6)^4 + 0.075 (x - 0.6)^3 - 12 (x - 2.85)^2 + 33.33 y^2 - \quad (23)$$

$$16 de(x, y, 1.4, 0, 2.51, 1.7) - 18.8 de(x, y, 2.3, 0, 2.51, 1.7) - 9.5 de(x, y, 3.35, 0, 2, 1.7) .$$

It is a global double minimum PES with some small dents corresponding to the bonds

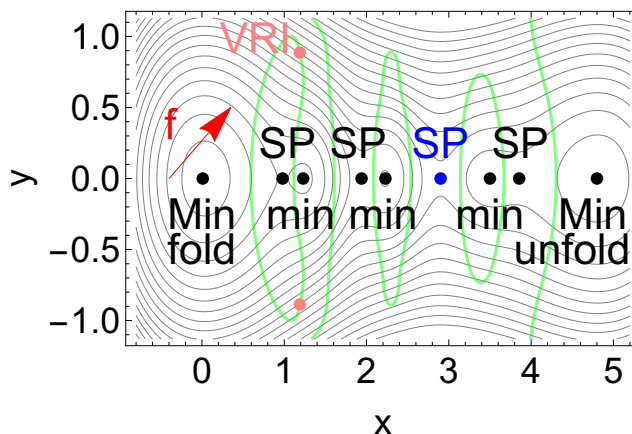


Figure 21: 2D section of the PES of the 4-base pair hairpin. x is the extension by the force, \mathbf{f} , however, y is globally a simple harmonic potential. The green curves are the BBP lines, and two VRI points are red. The global TS which we assume at the G-C pair¹¹² is depicted in blue. The force, \mathbf{f} , may point into the combined direction $(1.5, 1)^T$ to make the model not too simple. Note that the scaling of the axes is not equivalent.

between the single base pairs of the hairpin. This is shown in Fig. 21. x is the extension by the force, \mathbf{f} , of the end base pair $T - A$, however, y may be the collection of all other important coordinates of the unfolding process, like angle potentials, dihedrals, of even the bonds along the strands. The y -potential (outside the dents) is assumed by a harmonic ansatz for simplicity. Usually the folded form of a hairpin is the stable configuration, thus the PES has its global minimum here. The bonding potentials of the diverse base pairs are small, however, they combine by addition to a global TS at the G-C base pair.¹¹² It is depicted by a blue point in Fig. 21. The single base pairs may cause small intermediate minimums, depicted by the acronyms 'min' which, of course, also entail flat saddles. These intermediates are generated for the PES (23) by the three dent-functions of Eq.(22). The small minimum furthest to the left, for example, may describe the state that the first base pair, T-A, is open but the second pair, A-T, still holds the bonding. Such a state is possible, but of course, it is thermodynamically unstable.

We assume a force in the direction $\mathbf{f} = (1.5, 1)^T$. In a so-called hopping experiment¹¹³ the force goes over handles to the outer base pair, $T - A$, of the hairpin. For an amount of $F = 8.82$ to the direction $(0.832, 0.555)^T$ an equilibrium between the two states emerges here in our simple example. The populations of the folded and unfolded states are equal.¹¹⁴ In a hopping experiment, it is indicated by a 'global' 2-fold hopping of the extension between the two states, compare Fig. 2 of Ref.¹¹³ If we apply this force to the PES V_H , for simplicity by the ansatz of Eq.(1), ignoring that possibly the theory of NTs is questionable here, then we get the effective PES of Fig.22. There is included the NT along the given direction, by a black curve. On the NT the stationary points move, the NT is again the curve of the FDSPs: the folding minimum is destabilized, the blue global SP is strongly stabilized, the

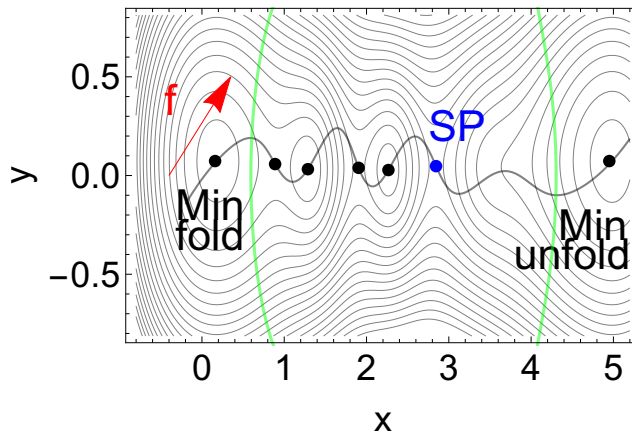


Figure 22: 2D section of the effective PES of the 4-base pair hairpin with $\mathbf{f} = 8.82(0.83, 0.56)^T$. The black curve is the NT to this direction. The global TS (blue) is still existent. The left and the right minima are still far away from the corresponding first, outer BBPs (green), compare Fig. 21. However, the fold- and unfold minima are now on the same level, compare Fig. 23.

intermediate furthest to the right disappeared, but the main effect is that the right minimum of the unfolded structure is strongly 'stabilized', it is now on the same level like the former global minimum,¹¹⁵ see Fig. 23.

We conclude that, at least in the case of hopping experiments, the main effect of the external force is the equilibration of the two minima of the two states of interest. Between these two states thermodynamic chemistry happens: transitions emerge here forwards and backwards, unfolding and refolding, on an equal rate, compare Fig. 2D of Ref.¹¹³ The effective global TS may influence the rate of these transitions. But it did not disappear, at the given amount of force. The corresponding BBPs on the NT are definitely not in the play; at least in this simplified example with only two 'global' minima. Note: diverse intermediates of the effective PES may cause that a single step between fold and unfold is divided into transition paths,¹¹⁴ however, that is not further discussed here. In contrast, one observes only one

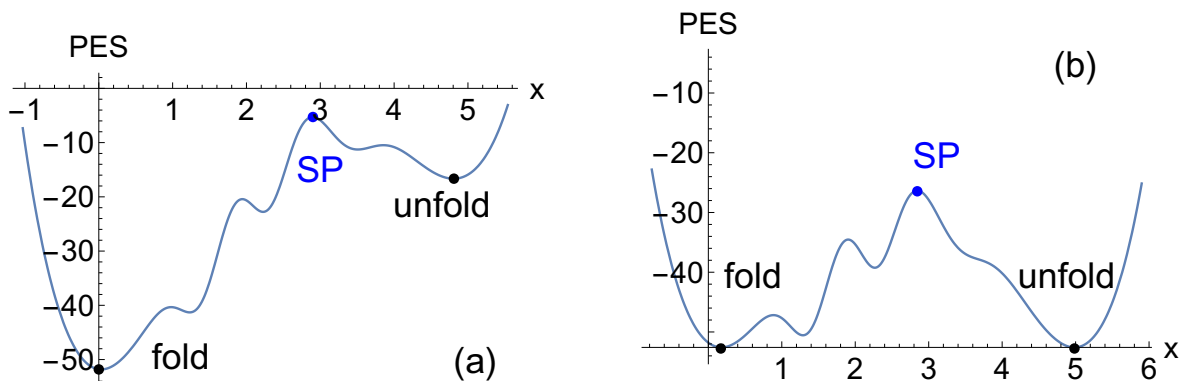


Figure 23: 1D section of the PES of the 4-base pair hairpin along the x -axis. (a) Profile on the original PES. The funnel-like shape of the curve is punctuated with small barriers and flat intermediate minima. (b) Profile on the effective PES to the given force.

rupture of the hairpin at high loading rates, in a corresponding experiment: all bonds can break in one burst.¹⁴

10 Discussion and conclusions

External force is an important way of probing regions of the PES that cannot be accessed by many other methods like temperature change, or change of concentration of the molecules, or change of the solutes. It should be repeated that under an external force with Eq.(1), the minima and TSs of the PES can move dramatically, and usually curvilinearly and not along a reaction coordinate, up to their flattening out in a shoulder at the critical force, \mathbf{f}_c . Thus, mechanical force is a remarkable effective stimulus of the activation of interesting reactions.¹⁴

We discussed the curvilinear behavior of the action of an external force to the curve of the FDSPs by very simple examples. For more complicated cases a tool was developed named 'force-matching force distribution analysis'.⁴⁷ But this misses the target here in this work. Our main point, and interest, is the understanding of the direction of a given external force, which decides which reaction valley on the PES is used for an induced reaction. To establish the relevance of our former works^{49,53,54,63,64,66,76} we go back here to the early beginnings of the pulling of very small molecular models. The model ansatz of Eqs.(1) and (2) allows to theoretically treat the influence of an external force, \mathbf{f} , on the PES of a molecule. Here we discuss this for the simplest three- and four-atomic molecules also using simple model potentials. We repeat the use of the theory of Newton trajectories (NTs) in the case of a fixed direction of the force in relation to the used coordinates. NTs describe in this case the behavior of the force-displaced stationary points (FDSPs). Note that the FDSPs are on a curve which is usually not the 'reaction coordinate' of the reaction of interest. Only if we apply an increasing force up to the critical one, \mathbf{f}_c , then the molecule can slide on the FDSPs curve, step by step, to the shoulder of the last effective PES. Then we can interpret the FDSPs curve as a kind of reaction coordinate. If the direction of the force changes along the pulling, in relation to the used coordinates, then the theory of NTs cannot be applied. But of course, by usual optimization procedures one can calculate for every force, \mathbf{f} , the corresponding FDSP for this force.

Sometimes one assumes, to explain molecular pulling experiments, that the force, \mathbf{f} , acts directly along a 'reaction coordinate' to reach the new, effective transition state of an induced reaction.²⁹ However, the simplest example in Section 3, of a linear triatomic ABC molecule, demonstrates that the end-to-end pulling already goes anywhere uphill on the PES between the two possible 'reaction coordinates' of the example. Thus the reality of every molecular pulling experiment will be quite more complicated than is assumed sometimes, see also the discussion in Ref.⁴⁴

Nevertheless, atomic-force microscopy and other methods^{116,117} of single molecules are a widely used tool to probe the bonds of molecules. There is a wide range, over many scales, from $0.01 pN$ to $1000 pN^2$ of the influence to a molecule. Very low forces up to $0.5 pN$ are needed for the sensing of weak strains.¹¹⁸ One uses $\approx 5 pN$ to flatten out the tertiary structure of peptides, their entropic elasticity.⁹⁶ Forces of a next higher order, $\approx 50 pN$, lead to opening of hairpins,^{14,74} supramolecular rearrangements, break down of H-bonds, and flattening out of weak local conformational dihedral angles,¹¹⁹ or protein-ligand interactions.⁷²

Biological machines also develop forces up to $60 pN$.^{41,64} At the next order of forces we can deform bond angles⁹⁶ (like in Section 5). At last, the next order of forces will break the weakest covalent bonds, like in Sections 3 and 4.

Given the lack of any electronic structure description of our simple models, we cannot compare here the definition of BBPs with other interesting special points on the reaction pathway like critical points of the electron density.^{120,121} Another interesting comparison could be the optimal BBP direction and the 'universal' coordinate proposed by the Boulatov group.⁷⁸ It should be a task for further treatments.

As mentioned and explained several times the use of force to activate chemical bonds and to initiate chemical reactions is of interest because the reaction pathways and outcome of mechanochemical reactions can be completely different from their thermal analogues.^{2,47} A very often mentioned example is the ring-opening reaction of cyclobutanes, an orbital controlled reaction, which has been extensively studied, computationally and experimentally.¹²² Thermal ring-opening is only allowed via a conrotatory pathway, yielding a different isomer of the ring-opened product (E,Z or E,E) for each starting isomer (cis- or trans-, respectively), the disrotatory pathway is forbidden, for a computational study see e.g. Ref.¹²³ Nevertheless, when the reaction is under an external mechanical force, the ring-opening always yields the E,E isomer as a product, irrespective of the starting material. The generic rationalization of this phenomenon is just exposed in Section 8. However, we have to take into account that the different outcomes of thermal and mechanochemical reactions are a direct consequence of the anisotropy of mechanical work involved in the force. In contrast to thermal energy, now the mechanical force has a direction. This is the basis of the mathematical theory exposed in Section 2.

In Section 4 we discussed the property that a polymer chain under sonication usually breaks at its center. Sijbesma et al.¹²⁴ describes a further, very interesting example of mechanochemistry corresponding to the evolution of the silver(I)-NHC bonds under forces. The description of the landscape obtained by these authors for this system is equivalent to that obtained using Eq. 1 as pointed out in Ref.,⁵³ compare Fig. 1 with Fig. 1 of Ref.⁸⁷ Another interesting and important point in mechanochemistry is also due to Sijbesma¹²⁵ being related to the theory discussed in the previous sections. Mechanochemical scission of covalent bonds in polymers is well-studied; in large molecules, forces on the molecule accumulate at the center of the chain to result in its midchain preferential scission. However, when one of the bonds in the chain is weaker, it selectively can break at this weaker bond. So a homolytic bond scission can be avoided.¹²⁶ Sijbesma et al.¹²⁵ demonstrated that this principle also holds for coordination bonds like ruthenium(II)-NHC. This fact can be related to the existence of optimal BBPs⁶⁶ whose effects are enhanced by this type of complexes. Note that we did not discuss here how fast the force is applied,^{14,106} because we treat only static properties of the effective PES.

Last but not least in Section 9, we found out that the most important property of the action of the drag force, \mathbf{f} , is the change of the relation between the reactant and a 'wished' product minimum. If any effective product minimum becomes deeper than the effective re-

actant then usual thermal chemistry happens: this reaction takes place. (If the TS is not too high for $k_B T$.)

Overall, the work shows that models of simple potential energy surfaces allow to rationalize a large body of experimental data in the field of mechanochemistry. Regardless of the simplicity of the models, general phenomena are predicted which should be proven experimentally.

Acknowledgements

WQ thanks Prof. William Hase for the stimulation to this paper on the WATOC 2017. Financial support from the Spanish Ministerio de Economía y Competitividad, Project CTQ2016-76423-P, and AGAUR Generalitat de Catalunya, Project 2017SGR348 is acknowledged. Thanks are due to a referee for hints to an earlier version.

References

1. Beyer, M. K.; Clausen-Schaumann, H. *Chem Rev* 2005, 105, 2921.
2. Caruso, M. M.; Davis, D. A.; Shen, Q.; Odom, S. A.; Sottos, N. R.; White, S. R.; Moore, J. S. *Chem Rev* 2009, 109, 5755.
3. Kaupp, G. *Cryst Eng Comm* 2009, 11, 388.
4. Kucharski, T. J.; Boulatov, R. *J Mater Chem* 2011, 21, 8237.
5. Ribas-Ariño, J.; Marx, D. *Chem Rev* 2012, 112, 5412.
6. Baláž, P.; Achimovičová, M.; Baláž, M.; Billik, P.; Cherkezova-Zheleva, Z.; Criado, J. M.; Delogu, F.; Dutková, E.; Gaffet, E.; Gotor, F. J.; Kumar, R.; Mitov, I.; Rojac, T.; Senna, M.; Streletskii, A.; Wiczorek-Ciurowa, K. *Chem Soc Rev* 2013, 42, 7571.
7. Wang, J.; Kouznetsova, T. B.; Niu, Z.; Ong, M. T.; Klukovich, H. M.; Rheingold, A. L.; Martinez, T. J.; Craig, S. L. *Nat Chem* 2015, 7, 323.
8. Subramanian, G.; Mathew, N.; Leiding, J. *JChemPhys* 2015, 143, 134109.
9. Makarov, D. E. *Single Molecule Science: Physical Principles and Models*; CRC Press, Taylor & Francis Group: Boca Raton, 2015.
10. Makarov, D. E. *J Chem Phys* 2016, 144, 030901.
11. Jha, S. K.; Brown, K.; Todde, G.; Subramanian, G. *JChemPhys* 2016, 145, 074307.
12. Zhuravlev, P. I.; Hinczewski, M.; Chakrabarti, S.; Marqusee, S.; Thirumalai, D. *Proc Natl Acad Sci* 2016, 113, E715.
13. Stauch, T.; Dreuw, A. *Chem Rev* 2016, 116, 14137.

14. Bo, G. D. *Chem Sci* 2018, 9, 15.
15. Spikes, H. *Friction* 2018, 6, 1.
16. Garcia-Manyes, S.; Beedle, A. E. M. *Nature Rev Chem* 2017, 1, 0083.
17. Gečiauskaitė, A. A.; Garcia, F. *Beilstein J Org Chem* 2017, 13, 2068.
18. Andre, V.; Quaresma, S.; Ferreira da Silva, J. L.; Duarte, M. T. *Beilstein J Org Chem* 2017, 13, 2416.
19. Quaresma, S.; Andre, V.; Fernandes, A.; Duarte, M. T. *Inorg Chim Acta* 2017, 455, 309.
20. Martina, K.; Manzoli, M.; Gaudino, E. C.; Cravotto, G. *Catalysts* 2017, 7, 98.
21. Rosen, B. M.; Percec, V. *Nature* 2007, 446, 381.
22. Lourderaj, U.; McAfee, J. L.; Hase, W. L. *J Chem Phys* 2008, 129, 094701.
23. Best, R. B.; Paci, E.; Hummer, G.; Dudko, O. K. *J Phys Chem B* 2008, 112, 5968 .
24. Grandbois, M.; Beyer, M.; Rief, M.; Clausen-Schaumann, H.; Gaub, H. E. *Science* 1999, 283, 1727.
25. Iozzi, M. F.; Helgaker, T.; Uggerud, E. *Mol Phys* 2009, 107, 2537.
26. Schmidt, S. W.; Kersch, A.; Beyer, M. K.; Clausen-Schaumann, H. *Phys Chem Chem Phys* 2011, 13, 5994.
27. Smalø, H. S.; Uggerud, E. *Mol Phys* 2013, 111, 1563.
28. Kedziora, G. S.; Barr, S. A.; Berry, R.; Moller, J. C.; Breitzman, T. D. *Theor Chem Acc* 2016, 135, 79.
29. Evans, E.; Ritchie, K. *BioPhys J* 1997, 72, 1541.
30. Kucharski, T. J.; Yang, Q.-Z.; Tian, Y.; Boulatov, R. *J Phys Chem Lett* 2010, 1, 2820.
31. Li, W.; Gräter, F. *J Am Chem Soc* 2010, 132, 16790.
32. Dopieralski, P.; Ribas-Ariño, J.; Anjukandi, P.; Krupicka, M.; Kiss, J.; Marx, D. *Nature Chem* 2013, 5, 685.
33. Stauch, T.; Dreuw, A. *Angew Chem Int Ed* 2016, 55, 811.
34. Stauch, T.; Dreuw, A. *Acc Chem Res* 2017, 50, 1041.
35. Ribas-Ariño, J.; Shiga, M.; Marx, D. *J Am Chem Soc* 2010, 132, 10609.
36. Tian, Y.; Boulatov, R. *Chem Phys Chem* 2012, 13, 2277.

37. Klukovich, H. M.; Kouznetsova, T. B.; Kean, Z. S.; Lenhardt, J. M.; Craig, S. L. *Nature Chem* 2013, 5, 110.
38. Eying, H.; Walter, J.; Rimball, G. E. *Quantum Chemistry*; John Wiley and Sons, Inc., New York, 1944.
39. Bell, G. I. *Science* 1978, 200, 618.
40. Garg, A. *Phys Rev B* 1995, 51, 15592.
41. Bustamante, C.; Chemla, Y. R.; Forde, N. R.; Izhaky, D. *Ann Rev Biochem* 2004, 73, 705.
42. Lin, H.-J.; Chen, H.-Y.; Sheng, Y.-J.; Tsao, H.-K. *Phys Rev Lett* 2007, 98, 088304.
43. Ong, M. T.; Leiding, J.; Tao, H.; Virshup, A. M.; Martínez, T. J. *J Am Chem Soc* 2009, 131, 6377.
44. Ribas-Ariño, J.; Shiga, M.; Marx, D. *Angew Chem, Int Ed* 2009, 48, 4190.
45. Wolinski, K.; Baker, J. *Molec Phys* 2009, 107, 2403 .
46. Schmidt, S. W.; Filippov, P.; Kersch, A.; Beyer, M. K.; Clausen-Schaumann, H. *ACS Nano* 2012, 6, 1314.
47. Li, W.; Edwards, S. A.; Lu, L.; Kubar, T.; Patil, S. P.; Grubmüller, H.; Groenhof, G.; Gräter, F. *ChemPhysChem* 2013, 14, 2687.
48. Avdoshenko, S. M.; Makarov, D. E. *J Phys Chem B* 2015, 120, 1537.
49. Quapp, W.; Bofill, J. M. *Int J Quantum Chem* 2018, 118, e25522.
50. Konda, S. S. M.; Brantley, J. M.; Bielawski, C. W.; Makarov, D. E. *J Chem Phys* 2011, 135, 164103.
51. Konda, S. S. M.; Avdoshenko, S. M.; Makarov, D. E. *J Chem Phys* 2014, 140, 104114.
52. Avdoshenko, S. M.; Makarov, D. E. *J Chem Phys* 2015, 142, 174106.
53. Quapp, W.; Bofill, J. M. *Theoret Chem Acc* 2016, 135, 113.
54. Quapp, W.; Bofill, J. M.; Ribas-Ariño, J. *JPhysChemA* 2017, 121, 2820.
55. Wolinski, K.; Baker, J. *Molec Phys* 2010, 108, 1845.
56. Quapp, W.; Hirsch, M.; Imig, O.; Heidrich, D. *J Comput Chem* 1998, 19, 1087.
57. Quapp, W.; Hirsch, M.; Heidrich, D. *Theor Chem Acc* 1998, 100, 285.
58. Bofill, J. M.; Anglada, J. M. *Theor Chem Acc* 2001, 105, 463.
59. Crehuet, R.; Bofill, J. M.; Anglada, J. M. *Theor Chem Acc* 2002, 107, 130.

60. Quapp, W. J *Theoret Comput Chem* 2003, 2, 385.
61. Pauling, L. *Chem Eng News* 1946, 24, 1375.
62. Friddle, R. W.; Noy, A.; Yoreo, J. J. D. *Proc Nat Acad Sci* 2012, 109, 13573.
63. Quapp, W.; Bofill, J. M. *J Comput Chem* 2016, 37, 2467.
64. Quapp, W. *J Math Chem* 2018, 56, 1339.
65. Kajdas, C. In *Tribology in engineering*; Pihtili, H., Ed.; InTech, 2013; p. 209.
66. Bofill, J. M.; Ribas-Ariño, J.; García, S. P.; Quapp, W. *JChemPhys* 2017, 147, 152710.
67. Maitra, A.; Arya, G. *Phys Chem Chem Phys* 2011, 13, 1836.
68. Smalø, H. S.; Rybkin, V. V.; Klopper, W.; Helgaker, T.; Uggerud, E. *J Phys Chem A* 2014, 118, 7683.
69. Dopieralski, P.; Ribas-Ariño, J.; Marx, D. *Angew Chem Int Ed* 2011, 50, 7105.
70. Hummer, G.; Szabo, A. *Proc Nat Acad Sci* 2001, 98, 3658.
71. Jarzynski, C. *Proc Nat Acad Sci* 2001, 98, 3636.
72. Van Patten, W. J.; Walder, R.; Adhikari, A.; Okoniewski, S. R.; Ravichandran, R.; Tinberg, C. E.; Baker, D.; Perkins, T. T. *ChemPhysChem* 2018, 19, 19.
73. Hyeon, C.; Thirumalai, D. *BioPhys J* 2006, 90, 3410.
74. Nunes-Alves, A.; Arantes, G. M. *J Chem Theory Comput* 2018, 14, 282.
75. Ray, S. S.; Ghosh, A.; Shit, A.; Chaudhuri, R. K.; Chattopadhyay, S. *Phys Chem Chem Phys* 2017, 19, 22282.
76. Quapp, W.; Bofill, J. M. *J Phys Chem B* 2016, 120, 2644.
77. Li, P.-C.; Makarov, D. E. *J Chem Phys* 2004, 121, 4826.
78. Akbulatov, S.; Tian, Y.; Huang, Z.; Kucharski, T. J.; Yang, Q.-Z.; Boulatov, R. *Science* 2017, 357, 299.
79. Garai, A.; Mogurampelly, S.; Bag, S.; Maiti, P. K. *J Chem Phys* 2017, 147, 225102.
80. Davis, D. A.; Hamilton, A.; Yang, J.; Cremer, L. D.; Gough, D. V.; Potisek, S. L.; Ong, M. T.; Braun, P.; Martínez, T.; White, S. R.; Moore, J. S.; Sottos, N. R. *Nature* 2009, 459, 68.
81. Bailey, A.; Mosey, N. J. *J Chem Phys* 2012, 136, 044102.
82. Hirsch, M.; Quapp, W. *J Molec Struct, THEOCHEM* 2004, 683, 1.

83. Lenhardt, J. M.; Black Ramirez, A. L.; Lee, B.; Kouznetsova, T. B.; Craig, S. L. *Macromolecules* 2015, 48, 6396.
84. Li, Y.; Niu, Z.; Burdynska, J.; Nese, A.; Zhou, Y.; Kean, Z. S.; Dobrynin, A. V.; Matyjaszewski, K.; Craig, S. L.; Sheiko, S. S. *Polymer* 2016, 84, 178.
85. Berkowski, K. L.; Potisek, S. L.; Hickenboth, C. R.; Moore, J. S. *Macromolecules* 2005, 38, 8975.
86. Kryger, M. J.; Munaretto, A. M.; Moore, J. S. *J Am Chem Soc* 2011, 133, 18992.
87. Groote, R.; Szyja, B. M.; Pidko, E. A.; Hensen, E. J. M.; Sijbesma, R. P. *Macromolecules* 2011, 44, 9187.
88. Wang, Q.; Gossweiler, G. R.; Craig, S. L.; Zhao, X. *J Mech Phys Sol* 2015, 82, 320.
89. Quapp, W.; Schmidt, B. *Theor Chem Acc* 2011, 128, 47.
90. Schmidt, B.; Quapp, W. *Theor Chem Acc* 2012, 132, 1305.
91. Maki, A.; Mellau, G.; Klee, S.; Winnewisser, M.; Quapp, W. *J Molec Spectr* 2000, 202, 67.
92. Diesendruck, C. E.; Zhu, L.; Moore, J. S. *Chem Commun* 2014, 50, 13235.
93. Beyer, M. K. *J Chem Phys* 2000, 112, 7307.
94. Makarov, D. E.; Wang, Z.; Thompson, J. B.; Hansma, H. G. *J Chem Phys* 2002, 116, 7760.
95. Chan, Y.; Haverkamp, R. G.; Hill, J. M. *J Theor Biol* 2010, 262, 498.
96. Oesterhelt, F.; Rief, M.; Gaub, H. E. *New J Phys* 1999, 1, 6.1.
97. Ghosal, A.; Cherayil, B. J. *J Chem Phys* 2018, 148, 094903.
98. Zhang, S.; Qi, S.; Klushin, L. I.; Skvortsov, A. M.; Yan, D.; Schmid, F. *J Chem Phys* 2018, 148, 044903.
99. Bustamante, C.; Marko, J. F.; Siggia, E. D.; Smith, S. *Science* 1994, 265, 1599.
100. Marko, J. F.; Siggia, E. D. *Macromolecules* 1995, 28, 8759.
101. Rief, M.; Grubmüller, H. *ChemPhysChem* 2002, 3, 255.
102. Haverkamp, R. G.; Williams, M. A. K.; Scott, J. E. *Bio-macromolecules* 2005, 6, 1816.
103. Iliafar, S.; Vezenov, D.; Jagota, A. *European Polymer J* 2014, 51, 151.
104. Dahlke, K.; Sing, C. E. *J Chem Phys* 2018, 148, 084902.
105. Quapp, W. *J Math Chem* 2015, 54, 137.

106. Rybkin, V. V. *J Phys Chem A* 2017, 121, 5758.
107. Nikitina, E.; Khavryutchenko, V. D.; Sheka, E. F.; Barthel, H.; Weis, J. *J Phys Chem A* 1999, 103, 11355.
108. Lupton, E. M.; Achenbach, F.; Weis, J.; Bräuchle, C.; Frank, I. *Phys Rev A* 2007, 76, 125420.
109. Smalø, H. S.; Uggerud, E. *Chem Commun* 2012, 48, 10443.
110. Xiao, B.; Zhang, H.; Johnson, R. C.; Marko, J. F. *Nucleic Acids Res* 2011, 39, 5568.
111. Hirsch, M.; Quapp, W. *J Math Chem* 2004, 36, 307.
112. Woodside, M. T.; Anthony, P. C.; Behnke-Parks, W. M.; Larizadeh, K.; Herschlag, D.; Block, S. M. *Science* 2006, 314, 1001.
113. Li, P. T. X.; Collin, D.; Smith, S. B.; Bustamante, C.; Tinoco Jr., I. *Biophys J* 2006, 90, 250.
114. Cossio, P.; Hummer, G.; Szabo, A. *J Chem Phys* 2018, 148, 123309.
115. Kirmizialtin, S.; Huang, L.; Makarov, D. E. *J Chem Phys* 2005, 122, 234915.
116. Neuman, K. C.; Nagy, A. *Nature Methods* 2008, 5, 491.
117. Makarov, D. E.; Schuler, B. *J Chem Phys* 2018, 148, 123001.
118. van de Laar, T.; Schuurman, H.; van der Scheer, P.; van Doorn, J. M.; van der Gucht, J.; Sprakel, J. *Chem* 2018, 4, 269.
119. Hyeon, C.; Thirumalai, D. *J Phys Cond Matt* 2007, 19, 113101.
120. Cremer, D.; Kraka, E. *Croat Chem Acta* 1984, 57, 1259.
121. Kraka, E.; Dunning Jr., T. H. In *Advances in Molecular Electronic Structure Theory: The Calculation and Characterization of Potential Energy Surfaces*; Dunning Jr., T. H., Ed.; JAI Press Inc., Greenwich, 1990; p. 129.
122. Ong, M. T.; Leiding, J.; Tao, H.; Virshup, A. M.; Martínez, T. J. *J Am Chem Soc* 2009, 131, 6377.
123. Quapp, W.; Bofill, J. M. *Int J Quantum Chem* 2015, 115, 1635.
124. Groote, R.; Jakobs, R. T. M.; Sijbesma, R. P. *Polymer Chem* 2013, 4, 4846.
125. Jakobs, R. T. M.; Sijbesma, R. P. *Organometallics* 2012, 31, 2476.
126. Shiraki, T.; Diesendruck, C. E.; Moore, J. S. *Faraday Discuss* 2014, 170, 385.